LETTER

doi:10.1038/nature12423

Vesicular and non-vesicular transport feed distinct glycosylation pathways in the Golgi

Giovanni D'Angelo[1,2], Takefumi Uemura[3], Chia-Chen Chuang[4], Elena Polishchuk[1], Michele Santoro[1], Henna Ohvo-Rekilä[5], Takashi Sato[3], Giuseppe Di Tullio[6], Antonio Varriale[2], Sabato D'Auria[2], Tiziana Daniele[6], Fabrizio Capuani[1], Ludger Johannes[7,8], Peter Mattjus[5], Maria Monti[9], Piero Pucci[9], Roger L. Williams[10], John E. Burke[10], Frances M. Platt[4], Akihiro Harada[3,11] & Maria Antonietta De Matteis[1]

Newly synthesized proteins and lipids are transported across the Golgi complex via different mechanisms whose respective roles are not completely clear. We previously identified a non-vesicular intra-Golgi transport pathway for glucosylceramide (GlcCer)—the common precursor of the different series of glycosphingolipids—that is operated by the cytosolic GlcCer-transfer protein FAPP2 (also known as PLEKHA8) (ref. 1). However, the molecular determinants of the FAPP2-mediated transfer of GlcCer from the *cis*-Golgi to the *trans*-Golgi network, as well as the physiological relevance of maintaining two parallel transport pathways of GlcCer—vesicular and non-vesicular—through the Golgi, remain poorly defined. Here, using mouse and cell models, we clarify the molecular mechanisms underlying the intra-Golgi vectorial transfer of GlcCer by FAPP2 and show that GlcCer is channelled by vesicular and non-vesicular transport to two topologically distinct glycosylation tracks in the Golgi cisternae and the *trans*-Golgi network, respectively. Our results indicate that the transport modality across the Golgi complex is a key determinant for the glycosylation pattern of a cargo and establish a new paradigm for the branching of the glycosphingolipid synthetic pathway.

Complex glycosphingolipids (GSLs), which have key roles in cell signalling, adhesion, proliferation and differentiation[2], are synthesized in the Golgi complex from GlcCer, which is synthesized from ceramide at the cytosolic leaflet of early Golgi membranes[3,4]. Upon translocation to the luminal leaflet, GlcCer is galactosylated to lactosylceramide (LacCer), which can then be converted into complex GSLs in later Golgi compartments (Fig. 1a)[5]. GlcCer can be transported through the Golgi complex via membrane trafficking and via non-vesicular transfer owing to the action of the cytosolic GlcCer-transfer protein FAPP2, which fosters GSL synthesis[1,6]. However, the respective roles of the vesicular and non-vesicular transport of GlcCer remain to be defined[7].

We have addressed this question by assessing the consequences of *FAPP2* gene ablation in mice (Fig. 1b–d and Supplementary Fig. 1a). *FAPP2*$^{-/-}$ mice showed no overt phenotype. However, measurement of GSL levels in the kidneys, where FAPP2 is highly expressed (Fig. 1b and Supplementary Fig. 1b), highlighted a specific decrease in the globoside series of GSL, in particular in globotriaosylceramide (Gb3), in *FAPP2*$^{-/-}$ mice (Fig. 1e). Visualization of GSLs using the Shiga toxin B fragment (ShTxB) that binds Gb3 (ref. 8), the cholera toxin B fragment (ChTxB) that binds monosialotetrahexosylganglioside (GM1) (ref. 9), and anti-monosialodihexosylganglioside (GM3) antibodies confirmed the previously reported distribution of Gb3 in the mouse kidney[10,11] and showed a selective reduction of Gb3 staining in the *FAPP2*$^{-/-}$ kidneys (Fig. 1f, g) and in kidney tubular cells isolated from *FAPP2*$^{-/-}$ mice (Supplementary Fig. 2).

Thus, FAPP2, in line with its rather recent evolutionary appearance coincident with the divergence of multiple GSL branches[12], selectively controls one GSL branch *in vivo*. We then performed the analysis of GSL in cells knocked down for *FAPP2* by short interfering RNA (siRNA) treatment (Supplementary Fig. 3). As reported previously[1], *FAPP2* knockdown induced a 40% decrease in the levels of total GSLs (taken as the sum of LacCer, GM3 and Gb3) but, considering the individual GSL species, it lowered the levels of LacCer and Gb3 but not GM3 (Fig. 2a). In agreement with these biochemical measurements, a selective decrease in ShTxB staining was also observed in *FAPP2* knockdown cells (Supplementary Fig. 4a).

When we analysed the impact of *FAPP2* knockdown on newly synthesized GSLs in ^{3}H-sphingosine-labelled HeLa cells, we found that FAPP2 depletion inhibited the synthesis of ^{3}H-LacCer and ^{3}H-Gb3 at all time points (Fig. 2b and Supplementary Fig. 4b). *FAPP2* knockdown, however, also inhibited the synthesis of ^{3}H-GlcCer at early time points, in agreement with previous results[1], and as a consequence lowered the levels of ^{3}H-GM3 (Fig. 2b and Supplementary Fig. 4b). To circumvent changes in complex GSLs that might be secondary to the inhibition of GlcCer synthesis, we bypassed GlcCer synthesis by labelling the cells with fluorescent GlcCer (C12 BODIPY-GlcCer). Under these conditions, FAPP2 depletion selectively inhibited the synthesis of C12-BODIPY-Gb3 but not of C12-BODIPY-GM3 (Fig. 2c), indicating that the decrease in Gb3 but not in GM3 synthesis was a direct consequence of FAPP2 depletion. Systematic silencing of enzymes involved in GSL biosynthesis (Figs 1a, 2d and Supplementary Fig. 4c, d) highlighted that the GSL profile induced by FAPP2 silencing was similar to that induced by LacCer synthase (LCS) silencing in terms of a decrease in LacCer, but they differed in their effects on downstream GSL species: LCS knockdown induced a uniform decrease in Gb3 and GM3 whereas *FAPP2* knockdown selectively decreased Gb3. These results indicate that the GlcCer transported via FAPP2 feeds a pool of LacCer specifically destined to globoside (that is, Gb3) synthesis. Dynamic assessment of GSL metabolic fluxes followed by mathematical modelling corroborated this conclusion (Supplementary Fig. 5).

To search for the mechanisms responsible for the different sensitivities of Gb3 and GM3 synthesis to FAPP2 depletion, we studied the intra-Golgi distribution of Gb3 synthase (Gb3S) and of GM3 synthase (GM3S) by two independent approaches[7]. First, we measured the synthesis of Gb3 and GM3 in cells treated with brefeldin A (BFA), a toxin that redistributes the Golgi cisternae (but not the *trans*-Golgi network (TGN)) into the endoplasmic reticulum (ER) (generating an ER–Golgi intermixed compartment), interrupts vesicular trafficking from this intermixed compartment to the TGN[13], and releases FAPP2 from Golgi membranes[14]. BFA treatment decreased the synthesis of Gb3

[1]Telethon Institute of Genetics and Medicine, Via Pietro Castellino 111, 80131 Naples, Italy. [2]Institute of Protein Biochemistry National Research Council, Via Pietro Castellino 111, 80131 Naples, Italy. [3]Laboratory of Molecular Traffic, Department of Molecular and Cellular Biology, Institute for Molecular and Cellular Regulation, Gunma University, Gunma 371-8512, Japan. [4]Department of Pharmacology, University of Oxford, Mansfield Road, Oxford OX1 3QT, UK. [5]Department of Biosciences, Biochemistry, Åbo Akademi University, Artillerigatan 6 A III, BioCity, FI-20520 Turku, Finland. [6]Department of Cell Biology and Oncology, Consorzio Mario Negri Sud, Via Nazionale 8/A, 66030 Santa Maria Imbaro, Chieti, Italy. [7]Institut Curie Centre de Recherche, 26 rue d'Ulm, 75248 Paris Cedex 05, France. [8]CNRS, UMR144, F-75248 Paris, France. [9]Dipartimento di Scienze Chimiche and CEINGE Biotecnologie Avanzate, Università di Napoli FedericoII, ViaGaetano Salvatore 482, 80145 Napoli, Italy. [10]MRC Laboratory of Molecular Biology, Hills Road, Cambridge CB2 0QH, UK. [11]Department of Cell Biology, Osaka University, Osaka 565-0871, Japan.

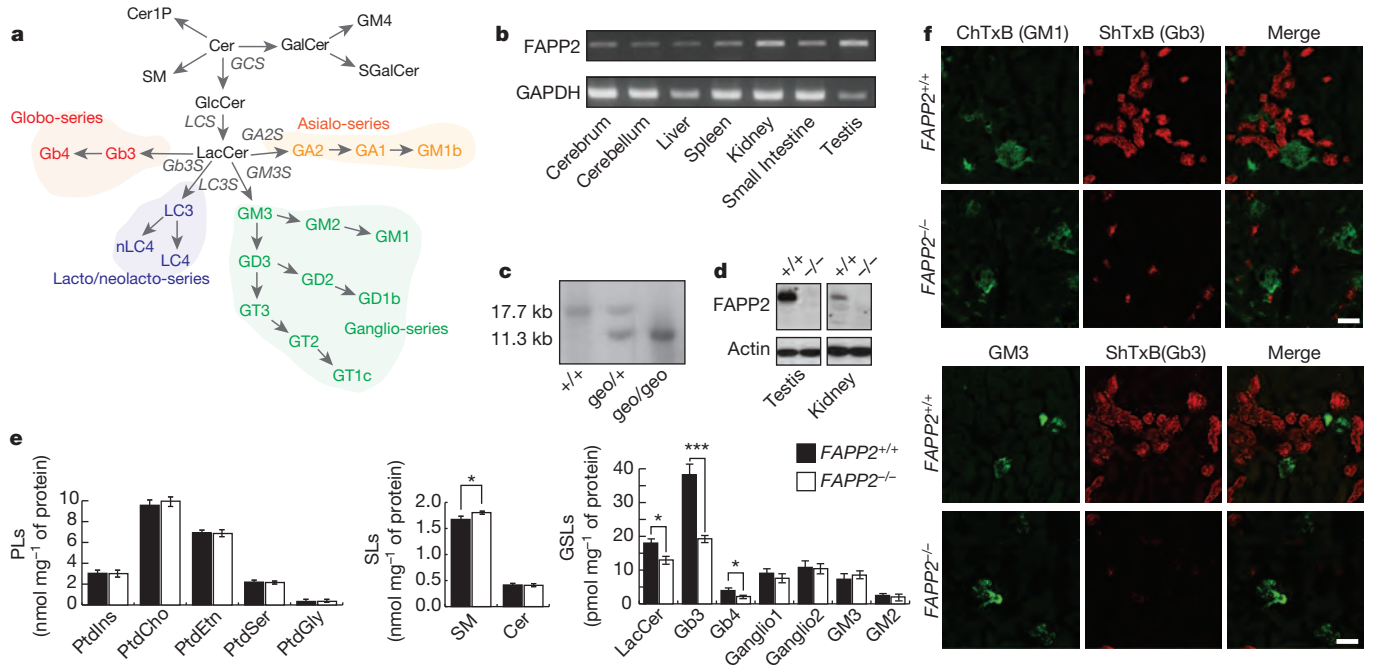

Figure 1 | FAPP2 selectively controls the levels of globosides *in vivo*. **a**, Simplified representation of the GSL synthetic pathway in vertebrates. GA2S, GA2 synthase; GCS, GlcCer synthase; LC3S, LC3 synthase. **b**, Expression of FAPP2 in mouse tissues. **c**, Southern blot of wild-type ($FAPP2^{+/+}$) and recombinant ($FAPP2^{geo/+}$ and $FAPP2^{geo/geo}$) mice tail DNA. See Supplementary Fig. 1b. **d**, FAPP2 levels in $FAPP2^{+/+}$ and $FAPP2^{-/-}$ testes and kidneys. **e**, Phospholipid (PL) and sphingolipid (SL) mass-spectrometry analysis, and GSL measurements of kidneys from $FAPP2^{+/+}$ ($n = 5$) and $FAPP2^{-/-}$ ($n = 10$) mice. Ganglio1, 2, unidentified gangliosides; Gb4, globoside; GM2, monosyalotrihexosylceramide; PtdCho, phosphatidylcholine; PtdIns, phosphatidylinositol; PtdEtn, phosphatidylethanolamine; PtdGly, phosphatidylglycine; PtdSer, phosphatidylserine; SM, sphingomyelin. Means ± s.e.m. **f**, ChTxB, ShTxB anti-GM3 staining of $FAPP2^{+/+}$ and $FAPP2^{-/-}$ kidney cortex sections. Representative pictures from at least five $FAPP2^{+/+}$ and five $FAPP2^{-/-}$ mice. Scale bars, 50 µm. $^{*}P < 0.05$; $^{***}P < 0.005$.

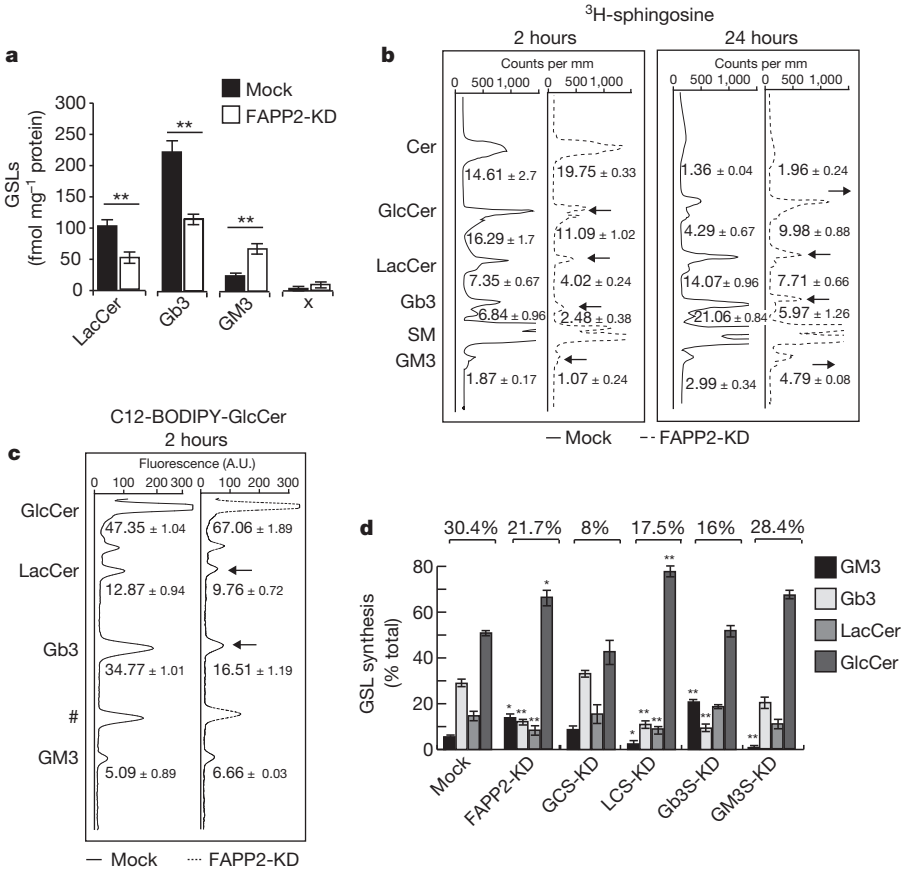

Figure 2 | FAPP2 is selectively required for Gb3 synthesis. **a**, GSL levels in HeLa cells. KD, knockdown; X, unassigned anionic GSL. **b**, High-performance thin-layer chromatography (HPTLC) profile of ^{3}H-sphingosine-labelled HeLa cells. Arrows denote changes induced by *FAPP2* knockdown. Numbers represent the percentage of each GSL species on total sphingolipids. **c**, HPTLC profile of C12-BODIPY-GlcCer-labelled HeLa cells. Arrows denote GSLs reduced by *FAPP2* knockdown; # represents unassigned peak and numbers represent the percentage of each GSL species on total GSL. A.U., arbitrary units. **d**, Effect of silencing of FAPP2 and of GSL synthetic enzymes on GSL species (expressed as percentage of total GSLs). Numbers represent the percentage of total GSLs on total sphingolipids. Means ± s.d. of at least three independent experiments. $^{*}P < 0.05$; $^{**}P < 0.01$.

but not that of GM3, indicating that the main fraction of endogenous Gb3S (but not of GM3S) resides in the TGN and thus remains segregated from its substrates that are synthesized in the BFA-induced intermixed ER–Golgi compartment (Fig. 3a). Second, we analysed the distribution of GM3S and Gb3S (Fig. 3b, c). In agreement with previous reports[6,15], we found that Gb3S is enriched in the TGN whereas GM3S is enriched in the Golgi cisternae. Moreover, consistent with its effect on GSL synthesis (Fig. 3a), BFA redistributed GM3S, but not Gb3S, to the ER (Supplementary Fig. 6).

The analysis of the role of FAPP2 was extended to other cell lines that also synthesize more complex gangliosides that, like GM3, were insensitive to FAPP2 depletion (Supplementary Fig. 7).

Thus, the synthesis of globosides at the TGN relies on the non-vesicular transport of GlcCer operated by FAPP2, whereas the synthesis of GM3 in the Golgi cisternae does not, eliciting the question as to whether GM3 synthesis depends instead on the vesicular transport of GlcCer. To address this question we inhibited intra-Golgi membrane trafficking[1] by treating cells with dicoumarol[1], by depleting the TRAPP component BET3 (also known as TRAPPC3) (ref. 1), or by depleting cytosolic phospholipase A_2 (cPLA$_2$) (ref. 16), and followed the transport of the temperature-sensitive mutant of vesicular stomatitis virus G protein (ts045-VSVG)[14]. As reported previously[1,16], these treatments suppressed the intra-Golgi progression of VSVG and strongly inhibited GM3 synthesis, but not Gb3 synthesis (Fig. 3d, e).

These results led us to propose that the vesicular transport of GlcCer feeds a pool of LacCer that is made in the Golgi cisternae and used for GM3 biosynthesis, whereas the non-vesicular transport of GlcCer via FAPP2 feeds a pool of LacCer that is made in the TGN and used in this compartment for globoside synthesis. This hypothesis generated some key predictions: (1) LCS should be present not only in the Golgi cisternae but also in the TGN; (2) other LacCer derivatives that, similarly to Gb3, are made at the TGN should depend on FAPP2; and (3) shifting the localization of GM3S from the Golgi cisternae to the TGN should make GM3 synthesis sensitive to FAPP2 depletion. We verified all of these predictions. First, LCS was found to localize both to the Golgi cisternae and to the TGN (Supplementary Fig. 8); second, *FAPP2* knockdown in SK-N-MC human neuronal cells selectively lowered the synthesis of gangliotriosylceramide (GA2), which is made in the TGN from LacCer (Fig. 1a and Supplementary Fig. 9a); third, GM3 synthesis, which is normally insensitive, becomes sensitive to FAPP2 depletion when a substantial fraction of GM3S is forced to localize at the TGN by expressing the enzyme at high levels (Supplementary Fig. 9b–d).

The selective requirement of FAPP2 for GSLs synthesized at the TGN, together with our previous observation that cells depleted of FAPP2 fail to concentrate GlcCer at the TGN[1], indicate that FAPP2 drives the transfer of GlcCer from the *cis*-Golgi—where GlcCer is synthesized—to the TGN, and raises the question of how this vectorial transport is sustained. We reasoned that in order to mediate the *cis*-Golgi-to-TGN transfer, apo-FAPP2 should be targeted to early Golgi membranes whereas GlcCer-bound FAPP2 should be targeted to the TGN. Thus, we compared the distribution of wild-type FAPP2 with that of a FAPP2 mutant, which is unable to bind GlcCer and thus is permanently apo (FAPP2(W407A))[1]. Although the main fraction of wild-type FAPP2 localizes at the TGN, the main fraction of FAPP2(W407A) localizes to the Golgi cisternae (Fig. 4a, b). Moreover, wild-type FAPP2 failed to localize at the TGN and was present mainly in the Golgi cisternae

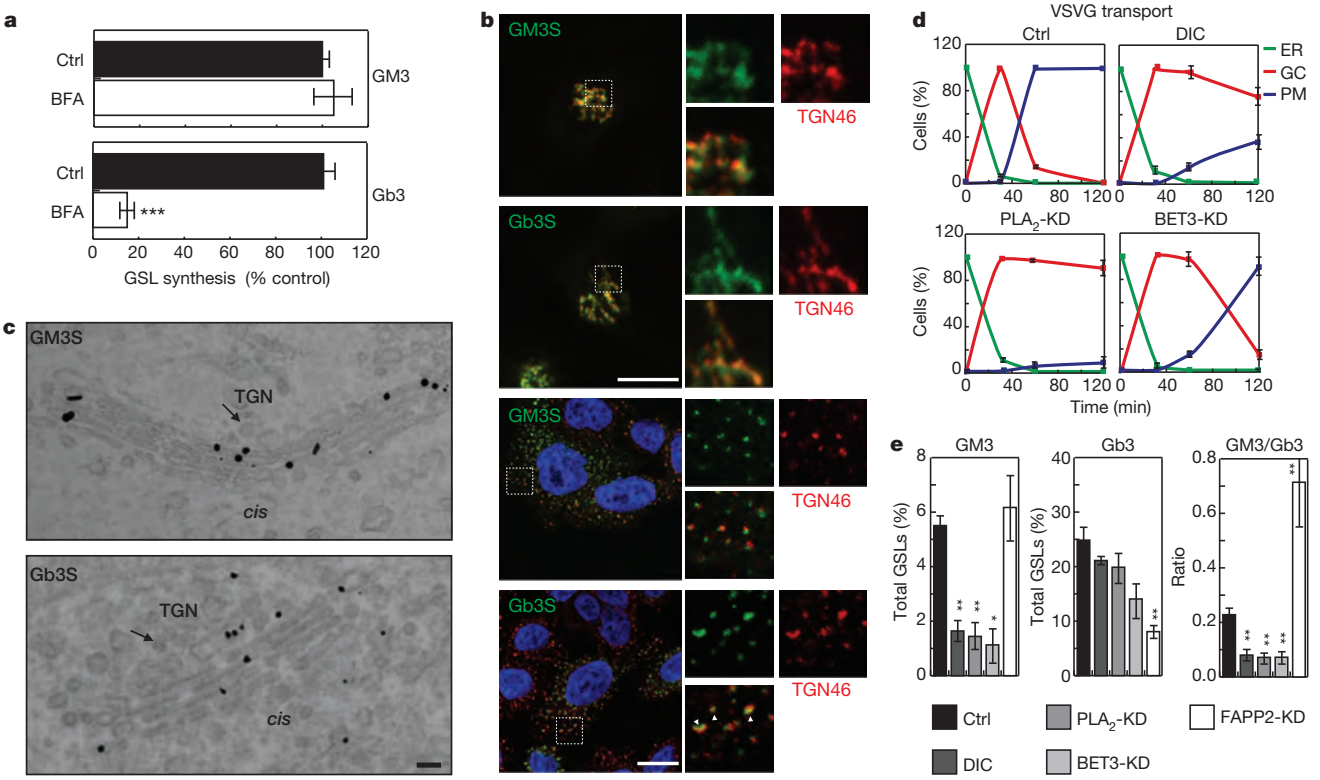

Figure 3 | Vesicular GlcCer transport feeds GM3 synthesis in the Golgi cisternae, whereas non-vesicular GlcCer transport feeds Gb3 synthesis in the TGN. **a**–**c**, Effect of BFA (5 μg ml^{-1}) on Gb3 and GM3 synthesis (**a**). Distribution of haemagglutinin (HA)–Gb3S and HA–GM3S evaluated by immunofluorescence (**b**) and by immunoelectron microscopy (**c**). In **b**, top panels represent untreated cells and bottom panels represent nocodazole-treated cells (3 h, 33 μM). Insets: enlargement of the boxed areas. The co-localization of HA–Gb3S and HA–GM3S with TGN46 was 50% and 14%, respectively. Data are representative of at least 30 cells per condition. Scale bar, 10 μm. **c**, Arrows represent clathrin-coated profiles at the TGN. Data are representative of at least 30 stacks. Scale bar, 100 nm. **d**, **e**, Effect of intra-Golgi trafficking blockage on VSVG transport (means ± s.d. in three independent experiments for at least 100 cells per time point) (**d**) and on GM3 and Gb3 synthesis (3-h ^{3}H-sphingosine pulse) (**e**). Means ± s.d. of three independent experiments. DIC, dicoumarol (200 μM); GC, Golgi complex; PM, plasma membrane. *$P < 0.05$; **$P < 0.01$; ***$P < 0.005$.

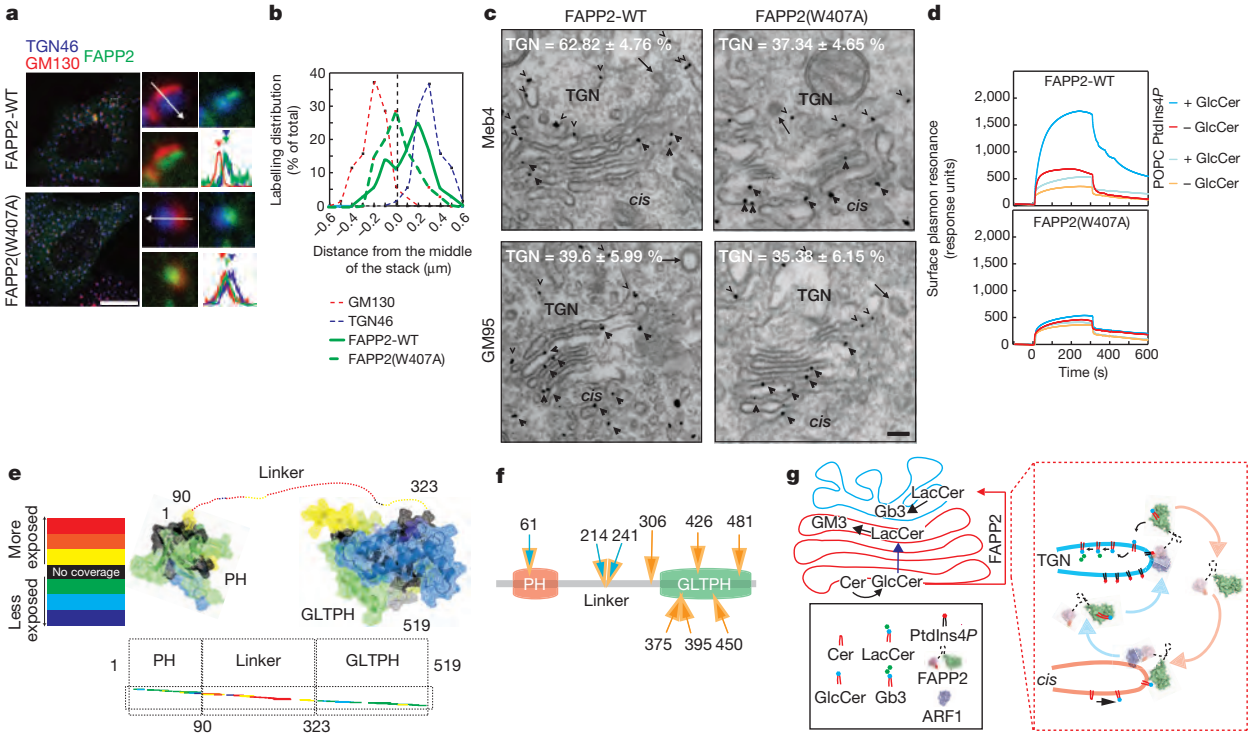

Figure 4 | GlcCer binding enhances the binding of FAPP2 to PtdIns4*P* and targets it to the TGN. **a**, Intra-Golgi distribution of wild-type FAPP2 (FAPP2-WT) and FAPP2(W407A) in nocodazole-treated cells (3 h, 33 μM). Right, enlargement of boxed areas and distribution of the maximal fluorescence intensity of FAPP2 along the *cis*-Golgi-to-TGN axis (white arrows). Scale bar, 10 μm. **b**, Quantification of the maximal labelling distribution of wild-type FAPP2 and FAPP2(W407A). The middle of the stack (0, black dashed line) is taken as a plane equidistant from GM130 and TGN46 fluorescence intensity peaks in 50 stacks per condition. **c**, Intra-Golgi distribution of wild-type FAPP2 and FAPP2(W407A) in Meb4 and GlcCer-deficient GM95 mouse cells. The percentage of TGN labelling is indicated. Means ± s.e.m. of at least 30 stacks per condition. Arrowheads represent Golgi cisternae staining, wedges represent TGN staining and arrows represent clathrin-coated profiles. Scale bar, 100 nm. **d**, Surface plasmon resonance analysis of the effect of GlcCer on FAPP2 binding to *1*-palmitoyl, *2*-oleoyl phosphatidylcholine (POPC)-PtdIns4*P* (98:2 mol:mol) liposomes. Results are representative of at least three independent experiments. PtdIns4*P* K_d value: 24 ± 0.9 μM for apo-FAPP2 and 6 ± 0.4 μM for GlcCer-bound FAPP2. **e**, Regions of FAPP2 showing different accessibility in HDX-MS were mapped on FAPP2. FAPP2 domains were modelled on the FAPP1 PH domain[18] and GLTPH domain[1,20]. **f**, Schematic representation of conformational changes induced by GlcCer loading on FAPP2 as assessed by HDX-MS (orange arrows) and controlled proteolysis-MS (blue arrows). Detailed results are presented in Supplementary Figs 12 and 13. **g**, Schematic representation of intra-Golgi non-vesicular (red arrow) and vesicular (blue arrow) transport of GlcCer. Inset: mechanism of FAPP2-mediated GlcCer-transfer directionality (cyan profiles, TGN; red profiles, Golgi cisternae; red arrows, targeting of apo-FAPP2 to the Golgi cisternae; cyan arrows, targeting of GlcCer-bound FAPP2 to the TGN.).

in cells that do not synthesize GlcCer[17], where FAPP2 is always apo (Fig. 4c). These results suggested that GlcCer binding positively regulates the targeting of FAPP2 to the TGN.

FAPP2 localization at the TGN is determined by its pleckstrin homology (PH) domain that coincidentally and independently[18] binds the small GTPase ARF1 and phosphatidylinositol 4-phosphate (PtdIns4*P*)[14], a phosphoinositide enriched at the TGN[19]. Single point mutations either in the PtdIns4*P*[14] or in the ARF-binding site[18] (Supplementary Fig. 10) abolish the recruitment of the PH domain to the Golgi complex (ref. 14 and data not shown), indicating a requirement for both binding sites. Interestingly, however, when these mutations are introduced into tandem forms of the FAPP PH-domain (di-PH), such that the di-PH has two binding sites either for ARF (di-PH-R18L) or for Ptdins4*P* (di-PH-E50A), the chimaeric proteins are able to localize to the Golgi complex, although with significantly different intra-Golgi distributions. In particular, a mutant FAPP-PH domain with a lower affinity for PtdIns4*P* and a higher affinity for ARF1 (di-PH-R18L) distributes throughout the Golgi stacks[14], whereas a mutant FAPP-PH domain with a lower affinity for ARF1 and a higher affinity for PtdIns4*P* (di-PH-E50A)[18] preferentially localizes to the TGN (Supplementary Fig. 10b), indicating that PtdIns4*P* dictates the TGN targeting of FAPP2.

We therefore assessed whether the preferential TGN association of GlcCer-bound FAPP2 could be due to the fact that it has a higher affinity for PtdIns4*P*. We found indeed that GlcCer loading (Supplementary information and Supplementary Fig. 11) increased FAPP2 binding to PtdIns4*P* (Fig. 4d), whereas it did not significantly affect the ability to bind ARF1 *in vitro* (not shown).

As FAPP2 binds GlcCer through its carboxy-terminal GLTP homology (GLTPH) domain[1,20] and PtdIns4*P* through its amino-terminal PH domain[14], the increase in PtdIns4*P* affinity induced by GlcCer binding suggested that GlcCer binding triggers a conformational change that is not limited to the GLTPH domain but is transmitted to more N-terminal regions. To gain insight into these conformational changes, we probed FAPP2 by hydrogen-deuterium exchange mass spectrometry (HDX-MS)[21]. The general profile of HDX-MS of FAPP2 indicated the presence of scarcely solvent-accessible N-terminal and C-terminal regions, corresponding to the PH-domain and the GLTPH domain, and the presence of a highly accessible and flexible intervening linker region (Fig. 4e). We then analysed the effects of GlcCer binding on the HDX-MS profile of FAPP2 and integrated this analysis with that of controlled proteolysis of FAPP2. The results of these analyses (Fig. 4f and Supplementary Figs 12 and 13) showed that the binding of GlcCer not only induced a stabilization of the GLTPH domain of FAPP2 but also affected the linker region interposed between the GLTPH domain and the PH domain, and on the PH domain itself, thus possibly having an impact on its PtdIns4*P* binding.

At this point a 'FAPP2 cycle' can be delineated (Fig. 4g): apo-FAPP2 associates with the *cis*-Golgi where it acquires GlcCer, resulting in a higher affinity of FAPP2 for PtdIns4*P*. FAPP2 then relocates to the PtdIns4*P*-enriched TGN where it delivers GlcCer.

Our findings establish a new paradigm for GSL biosynthesis whereby two branches receive their common precursor, GlcCer, from two parallel transport routes (Fig. 4g): the vesicular route feeds the LacCer pool used to make the ganglio-series in the Golgi cisternae, whereas the non-vesicular route mediated by FAPP2, which bypasses the intervening cisternae and delivers GlcCer to the TGN, feeds a TGN pool of LacCer converted *in loco* into GSLs of the globo- or asialo-series (Figs 1a and 4g). In a wider context, our results show how different modes of transporting a cargo through the Golgi complex channel the cargo itself towards distinct and otherwise potentially competing glycosylation pathways.

METHODS SUMMARY

FAPP2$^{-/-}$ mice were obtained following the procedure described in Supplementary Data and in ref. 22. High-performance liquid chromatography-based GSL measurements, metabolic labelling with ^{3}H-sphingosine, GSL extraction and HPTLC and analysis, as well as immunofluorescence and immunoelectron microscopy studies for subcellular protein localization assessments, were performed as described in ref. 1. Transport of ts045-VSVG was assessed as described previously[23]. Protein purification, fluorescence, circular dichroism and surface plasmon resonance studies were performed as described in refs 24, 25. HDX-MS was performed as in ref. 26. For statistical analysis, two-tailed Student *t*-tests were applied to the data. $*P < 0.05$; $**P < 0.01$; $***P < 0.005$.

Full Methods and any associated references are available in the online version of the paper.

Received 21 June 2012; accepted 25 June 2013.
Published online 4 August 2013.

1. D'Angelo, G. *et al.* Glycosphingolipid synthesis requires FAPP2 transfer of glucosylceramide. *Nature* **449,** 62–67 (2007).
2. Hakomori, S. I. Structure and function of glycosphingolipids and sphingolipids: recollections and future trends. *Biochim. Biophys. Acta* **1780,** 325–346 (2008).
3. Jeckel, D., Karrenbauer, A., Burger, K. N., van Meer, G. & Wieland, F. Glucosylceramide is synthesized at the cytosolic surface of various Golgi subfractions. *J. Cell Biol.* **117,** 259–267 (1992).
4. Futerman, A. H. & Pagano, R. E. Determination of the intracellular sites and topology of glucosylceramide synthesis in rat liver. *Biochem. J.* **280,** 295–302 (1991).
5. Hannun, Y. A. & Obeid, L. M. Principles of bioactive lipid signalling: lessons from sphingolipids. *Nature Rev. Mol. Cell Biol.* **9,** 139–150 (2008).
6. Halter, D. *et al.* Pre- and post-Golgi translocation of glucosylceramide in glycosphingolipid synthesis. *J. Cell Biol.* **179,** 101–115 (2007).
7. Maccioni, H. J., Quiroga, R. & Ferrari, M. L. Cellular and molecular biology of glycosphingolipid glycosylation. *J. Neurochem.* **117,** 589–602 (2011).
8. Jacewicz, M., Clausen, H., Nudelman, E., Donohue-Rolfe, A. & Keusch, G. T. Pathogenesis of shigella diarrhea. XI. Isolation of a shigella toxin-binding glycolipid from rabbit jejunum and HeLa cells and its identification as globotriaosylceramide. *J. Exp. Med.* **163,** 1391–1404 (1986).
9. van Heyningen, S. V. Cholera toxin: interaction of subunits with ganglioside G_{M1}. *Science* **183,** 656–657 (1974).
10. Psotka, M. A. *et al.* Shiga toxin 2 targets the murine renal collecting duct epithelium. *Infect. Immun.* **77,** 959–969 (2009).
11. Okuda, T. *et al.* Targeted disruption of Gb3/CD77 synthase gene resulted in the complete deletion of globo-series glycosphingolipids and loss of sensitivity to verotoxins. *J. Biol. Chem.* **281,** 10230–10235 (2006).
12. D'Angelo, G., Vicinanza, M. & De Matteis, M. A. Lipid-transfer proteins in biosynthetic pathways. *Curr. Opin. Cell Biol.* **20,** 360–370 (2008).
13. Chege, N. W. & Pfeffer, S. R. Compartmentation of the Golgi complex: brefeldin-A distinguishes trans-Golgi cisternae from the trans-Golgi network. *J. Cell Biol.* **111,** 893–899 (1990).
14. Godi, A. *et al.* FAPPs control Golgi-to-cell-surface membrane traffic by binding to ARF and PtdIns(4)P. *Nature Cell Biol.* **6,** 393–404 (2004).
15. Yamaji, T., Nishikawa, K. & Hanada, K. Transmembrane BAX inhibitor motif containing (TMBIM) family proteins perturbs a *trans*-Golgi network enzyme, Gb3 synthase, and reduces Gb3 biosynthesis. *J. Biol. Chem.* **285,** 35505–35518 (2010).
16. San Pietro, E. *et al.* Group IV phospholipase $A_2\alpha$ controls the formation of inter-cisternal continuities involved in intra-Golgi transport. *PLoS Biol.* **7,** e1000194 (2009).
17. Ichikawa, S., Nakajo, N., Sakiyama, H. & Hirabayashi, Y. A mouse B16 melanoma mutant deficient in glycolipids. *Proc. Natl Acad. Sci. USA* **91,** 2703–2707 (1994).
18. He, J. *et al.* Molecular basis of phosphatidylinositol 4-phosphate and ARF1 GTPase recognition by the FAPP1 pleckstrin homology (PH) domain. *J. Biol. Chem.* **286,** 18650–18657 (2011).
19. D'Angelo, G., Vicinanza, M., Di Campli, A. & De Matteis, M. A. The multiple roles of PtdIns(4)*P*–not just the precursor of PtdIns(4,5)*P*2. *J. Cell Sci.* **121,** 1955–1963 (2008).
20. Kamlekar, R. K. *et al.* The glycolipid transfer protein (GLTP) domain of phosphoinositol 4-phosphate adaptor protein-2 (FAPP2): structure drives preference for simple neutral glycosphingolipids. *Biochim. Biophys. Acta* **1831,** 417–427 (2013).
21. Yan, X., Watson, J., Ho, P. S. & Deinzer, M. L. Mass spectrometric approaches using electrospray ionization charge states and hydrogen-deuterium exchange for determining protein structures and their conformational changes. *Mol. Cell. Proteomics* **3,** 10–23 (2004).
22. Sato, T. *et al.* The Rab8 GTPase regulates apical protein localization in intestinal cells. *Nature* **448,** 366–369 (2007).
23. D'Angelo, G. *et al.* GRASP65 and GRASP55 sequentially promote the transport of C-terminal valine-bearing cargos to and through the Golgi complex. *J. Biol. Chem.* **284,** 34849–34860 (2009).
24. Zhai, X. *et al.* Glycolipid acquisition by human glycolipid transfer protein dramatically alters intrinsic tryptophan fluorescence: insights into glycolipid binding affinity. *J. Biol. Chem.* **284,** 13620–13628 (2009).
25. Ohvo-Rekilä, H. & Mattjus, P. Monitoring glycolipid transfer protein activity and membrane interaction with the surface plasmon resonance technique. *Biochim. Biophys. Acta* **1808,** 47–54 (2011).
26. Burke, J. E., Perisic, O., Masson, G. R., Vadas, O. & Williams, R. L. Oncogenic mutations mimic and enhance dynamic events in the natural activation of phosphoinositide 3-kinase p110alpha (*PIK3CA*). *Proc. Natl Acad. Sci. USA* **109,** 15259–15264 (2012).

Supplementary Information is available in the online version of the paper.

Acknowledgements We thank A. Luini, C. Wilson and D. Priestman for discussions, A. Egorova for help with electron microscopy, G. Liebisch, A. Sigruener and G. Schmitz for lipidomic analysis. M.A.D.M. acknowledges the support of Telethon (GSP08002 and GGP06166), Associazione Italiana per la Ricerca sul Cancro (AIRC) (IG 8623), and the EU (FP7 Lipidomicnet). G.D.'A. acknowledges the support of AIRC (MFAG 10585). P.M. acknowledges the support of Academy of Finland and Sigrid Jusélius Foundation. C.-C.C. was funded by a Study Abroad Scholarship from the Taiwan Ministry of Education.

Author Contributions M.A.D.M. supervised the entire project; M.A.D.M. and G.D.'A. wrote the manuscript with comments from all co-authors; G.D.'A., with the help of M.S., designed and conducted at TIGEM the experiments of sphingolipid labelling, membrane trafficking, immuno-localization and controlled proteolysis. M.S. designed the strategy and produced plasmid vectors. M.S. and G.D.T. prepared recombinant proteins, anti-FAPP2 and anti-BET3 antibodies. T.U. and T.S. generated and characterized *FAPP2*$^{geo/geo}$ and *FAPP2*$^{-/-}$ mice under the supervision of A.H. C.-C.C. conducted the HPLC measurements of GSLs under the supervision of F.M.P. L.J. provided the Cy3-ShTxB. E.P. and T.D. conducted the electron microscopy experiments. H.O.-R. conducted the surface plasmon resonance experiments under the supervision of P.M. A.V. conducted the tryptophan fluorescence and circular dichroism experiments under the supervision of S.D'.A. F.C. and G.D'.A. produced the mathematical model for GSL metabolism. M.M. and P.P. performed and interpreted the MS analysis; R.L.W. and J.E.B. performed and interpreted the HDX analysis.

Author Information Reprints and permissions information is available at www.nature.com/reprints. The authors declare no competing financial interests. Readers are welcome to comment on the online version of the paper. Correspondence and requests for materials should be addressed to M.A.D.M. (dematteis@tigem.it).

METHODS

Reagents and antibodies. All chemical reagents were of analytical grade or higher and purchased from Sigma unless otherwise specified. Cell culture media were from Invitrogen. Polyclonal antibodies against human FAPP2, BET3, cPLA$_2$IVa and GM130 were raised in rabbits using glutathione *S*-transferase fusion proteins as immunogens. All were affinity purified on their corresponding immunogens. The anti-VSVG clone P5D4, anti-Flag M2 and anti-HA monoclonal antibodies, and the anti-rabbit and anti-mouse IgG Cy3-conjugated antibodies were from Sigma. The Alexa 488-conjugated ChTxB fragment was from Invitrogen. The Cy3-conjugated ShTxB fragment was prepared as described[27]. The mouse monoclonal antibody against GM3 (clone 2590) was from Cosmo Bio Co. Sheep polyclonal antibodies against TGN46 were from AbD Serotech. The Alexa 488 goat anti-mouse and anti-rabbit IgG antibodies were from Molecular Probes. All unlabelled purified lipids were from Avanti Polar Lipids. ^{3}H-sphingosine was from PerkinElmer. Stock solutions of GSLs were prepared in chloroform/methanol (2:1 by volume) and of other lipids in hexane/2-propanol (3:2 by volume). Lipid solutions were stored in the dark at $-20\,^{\circ}$C and warmed to room temperature before use.

FAPP2 Knockout mice. Mice were from the C57BL/6 strain. All animal procedures were performed in accordance with the guidelines of the Animal Care and Experimentation Committee of Gunma University, and all animals were bred in the Institute of Animal Experience Research of Gunma University. *FAPP2* knockout mice were generated following the procedure described in Supplementary information. Histological, immunofluorescence microscopy and X-gal staining were performed as previously described[22,28,29].

Cell culture. HeLa, Meb4, GM95, HepG2, HK2, COS7 and MDCK cells were grown and transiently transfected by TransIT-LT1 (Mirus Bio) as described in ref. 1. Stably-expressing HeLa-GM3S cells were obtained after transfection of the 3×HA–GM3S coding plasmid and selection in the presence of G418 (Invitrogen) and screening of monoclonal colonies by indirect immunofluorescence.

Plasmids and constructs. Most of the constructs used in this study were obtained from HeLa RNA by RT–PCR and cloning into appropriate vectors. In brief, total RNA was isolated from HeLa cells; RT–PCR was performed using a poly dT oligo as a primer. The complementary DNA obtained was used as a template for PCR, using the following primers: for Gb3S: forward 5′-GTTGAATTCGATCTGG GGATACCATGTCC-3′, reverse 5′-CACCTCGAGCAAGTACATTTTCATGG CCTC-3′; for GM3S: forward 5′-CAGGAATTCAGAATGAGAAGGCCCA GCTTGTTA-3′, reverse 5′-AACGCGGCCGCTGAAATTCACGATCAATGC CTCCA-3′; for LCS: forward 5′-ATAGAATTCTGGCTGCAGCATGCGCGC-3′, reverse 5′-CGCGATATCAAGTACTCGTTCACCTGAGCCA-3′. The PCR products were cloned into a linearized pCR2.1 vector, and processed for automatic sequencing. All of the cloned sequences matched the sequence reported in databases for human Gb3S (AF513325), GM3S (AY152815.2) and LCS (B4GALT5; (NM_004776)). The DNAs corresponding to the various coding sequences were then subcloned into EcoRI/XhoI (Gb3S), EcoRI/NotI (GM3S), EcoRI/EcoRV sites of pCDNA3-3XHA at C-terminus or p3XFLAG-CMV-14.

Green fluorescent protein (GFP)–FAPP2 wild-type and W407A constructs were obtained as described in ref. 1; recombinant GST–FAPP2 wild-type, GST–FAPP2(W407A), His-FAPP2 wild type and His-FAPP2(W407A) were produced in *Escherichia coli* as described in ref. 1.

GFP–diFAPP2PH-wild type and E50A were obtained as follows: GFP–FAPP2 wild-type DNA was used as a template for two distinct PCR reactions using as primers: PCR (a): 5′-TCTGAATTCATGGAGGGGGTGCTGTACA-3, 5′-TAT GGTACCGAGCAAGCAAGCCTTGGCTGATCCC-3; PCR (b): 5′-TATGGT ACCTTGCTGGAGGGGGTGCTGTACAAGTG-3, 5′-TCACTCGAGTTAGCA AGCCTTGGCTGATCC-3. Products from PCR (a) were subcloned into EcoRI/KpnI sites of vector pEGFP-C1 to obtain construct pEGFP-FAPP2PH. Subsequently, products from PCR (b) were subcloned into KpnI/XhoI sites of the pEGFP-FAPP2PH construct to obtain GFP–diFAPP2PH-wild type. A similar procedure was applied to obtain the GFP–diFAPP2PH(E50A) mutant using as a template GFP–FAPP2(E50A) DNA. GFP–FAPP2(E50A) was obtained from wild-type GFP–FAPP2 by site-directed mutagenesis using the primers 5′-GAGCATACAAATGGCAGTCTGTGCAATTCAAGTTCATTCTGTAG-3′ and 5′-CTACAGAATGAACTTGAATTGCACAGACTGCCATTTGTATGCTC-3′.

siRNA treatments. The siRNAs for human FAPP2 (NM_001197026), GCS (NM_003358), BET3 (NM_014408), B4GALT5 (NM_004776), B4GALT6 (NM_004775), SIAT9/GM3S (AY152815.2), A4GALT/Gb3S (NM_017436), PLA$_2$ (NM_001199562) comprised mixtures of at least three siRNA duplexes (Supplementary Table 1) and were obtained from Dharmacon. HeLa, HK2, HepG2 and MDCK cells were plated at 30% confluence in 12-well plates and transfected with 120–150 pmol of siRNAs with Oligofectamine (Invitrogen) or Dharmafect4 (Dharmacon), in accordance with the manufacturer's protocol. At 72 h after the initial treatment with siRNA, the cells were processed directly. Silencing efficiency was evaluated either by western blot (Supplementary Fig. 2) or by quantitative PCR (Supplementary Fig. 4b) using specific primers (Supplementary Table 1).

Measurement of GSLs. Metabolic labelling with ^{3}H-sphingosine or ^{14}C-galactose, GSL extraction and HPTLC and analysis were performed as described in refs 1, 6.

Immunofluorescence and morphometric analysis. All immunofluorescence experiments were performed as described previously[1,14]. Images are confocal optical slices obtained using an LSM 710 (Zeiss) confocal microscope. Co-localization analysis was performed as described in ref. 14 or by using an object-based co-localization method included in the JACoP v2.0 application for ImageJ[30]. In brief, individual mini-stacks in nocodazole-treated cells were considered as objects whose mass-centre position was calculated after segmentation. The perfect coincidence of mass-centre positions for two distinct labellings (that is, Gb3S/TGN46 or GM3S/TGN46) in a single mini-stack was considered as a positive co-localization event.

Immunoelectron microscopy. Immunoelectron microscopy was performed in transfected HeLa, Meb4 and GM95 cells as described previously[1].

VSVG intracellular transport assay. Transport of ts045-VSVG was assessed as described previously[23].

Statistical analysis. For statistical analysis, two-tailed Student *t*-tests were applied to the data. $*P < 0.05$; $**P < 0.01$; $***P < 0.005$.

27. Mallard, F. & Johannes, L. Shiga toxin B-subunit as a tool to study retrograde transport. *Methods Mol. Med.* **73,** 209–220 (2003).
28. Muramatsu, K. *et al.* Neuron-specific recombination by Cre recombinase inserted into the murine *tau* locus. *Biochem. Biophys. Res. Commun.* **370,** 419–423 (2008).
29. Hashimoto, Y. *et al.* Neuron-specific and inducible recombination by Cre recombinase in the mouse. *Neuroreport* **19,** 621–624 (2008).
30. Bolte, S. & Cordelieres, F. P. A guided tour into subcellular colocalization analysis in light microscopy. *J. Microsc.* **224,** 213–232 (2006).

doi:10.1038/nature12423

Supplementary data

Establishing FAPP2 Knockout mice

We used a previously described knockout system[22] to generate the FAPP2-/- mice. Briefly, the *FAPP2* gene was isolated from a mouse genomic BAC library derived from the 129Sv/J mouse strain (RPCI-22: Children's Hospital, Oakland Research Institute). An FRT-flanked SA-IRES-β-geo-polyA cassette was introduced into intron 4 and a loxP site was introduced into intron 3 in the FAPP2 targeting vector (**Supplementary Fig.1**). Recombinant ES cell clones were identified and heterozygous mice (FAPP2geo/+) were generated. By crossing the geo/+ mice with transgenic mice that ubiquitously express Flp recombinase, the SA-IRES-β-geo-polyA cassette is expected to be excised (flox/flox) and the expression of the gene will be recovered. We used the resulting flox/flox mice to generate conditional FAPP2 knockouts by crossing them with Cre transgenic mice.

The following primers were used for genotyping by PCR analysis:

5'- GTGCAGGCTGATACGATACTGCAGA-3' (Primer 1),

5'-GGATCAAGGCGATGACGTGGATTTC-3' (Primer 2),

5'-CCGTACAGTTCCACAAAGGCATCCT -3' (Primer 3),

5'-TGGCTGCAGAGCCTTGCTGGTAATG -3' (Primer 4),

5'-GTCCCCGGTGATGCTGTGATTGTGA -3' (Primer 5).

Primers 1 and 2 detected the *FAPP2* wild-type allele, primers 1 and 3 detected the geo allele of *FAPP2*, and primers 4 and 5 detected the null allele of *FAPP2*.

To confirm that FAPP2 is not expressed in the *FAPP2-/-* mice, we performed Western blot using FAPP2-specific antibodies. FAPP2 proteins were not detected in crude extracts from *FAPP2 -/-* mice (**Fig. 1c**).

RNA isolation and RT-PCR: Total RNA was extracted from organs from adult mice by a phenol/chloroform extraction procedure using RNAiso (Takara). 3 μg of total RNA was primed with oligo(dT) to synthesize first-strand cDNA with reverse transcriptase. The primers used for PCR were as follows:

FAPP2 sense primer: 5'-CTCGCATGGACCTCATCATC-3',

FAPP2 antisense primer: 5'-GATGCTGCAATCCACCTCTG-3',
GAPDH sense primer: 5'- ACCACAGTCCATGCCATCAC-3',
GAPDH antisense primer: 5'- TCCACCACCCTGTTGCTGTA-3'.

Flux analysis and mathematical modelling of GSL synthesis

To assess the SL metabolic fluxes, we pulsed FAPP2-KD cells and mock-treated HeLa cells for 2 h with ^{3}H-sphingosine followed by a chase for 0, 2, 6, and 24 h (**Supplementary Fig. 4b**). The rates of Cer consumption and SM production in FAPP2-KD cells were comparable to control cells, although the overall SM levels were significantly higher at all time points. As previously reported[1], GlcCer levels were lower in FAPP2-KD cells at the early time points, possibly due to a product-inhibition effect of GlcCer on GCS as a consequence of impaired GlcCer consumption that, indeed, accumulates over time. Interestingly, while Gb3 and LacCer synthesis were inhibited in FAPP2-KD cells, GM3 synthesis was not. The above analysis indicated that FAPP2 depletion induces a complex rearrangement of GSL metabolism, raising the question as to whether this rearrangement was a direct consequence of impaired GlcCer transport or whether additional effects should be envisaged. To address this question we built a mathematical model based on the experimental data shown in **Supplementary Fig. 4b**. We modelled GSL reactions as first-order reactions, by means of Ordinary Differential Equations (ODE), following the law of mass action. We considered different conditions in which FAPP2 depletion alternatively affected the reaction rates (k_1 to k_5) corresponding to the synthetic steps leading from Cer to SM (k_1), from SM to Cer (k_{1R}), from Cer to GlcCer (k_2), from GlcCer to LacCer (k_3), from LacCer to Gb3 (k_4) or to GM3 (k_5). We also introduced k_{3A} and k_{3B} as reaction rates leading to the two pools of LacCer (LacCerA and LacCerB) destined for the synthesis of Gb3 and GM3, respectively (**Supplementary Fig. 5a**). The ODEs for GSL conversion read:

$$\frac{dCer}{dt} = -k_1 Cer + k_{1R} SM - k_2 Cer$$

$$\frac{dGlcCer}{dt} = k_2 Cer - (k_3 + k_{3A} + k_{3B}) GlcCer$$

$$\frac{dLacCer_A}{dt} = k_{3A} GlcCer - k_4 LacCer_A$$

$$\frac{dLacCer_B}{dt} = k_{3B} GlcCer - k_5 LacCer_B$$

$$\frac{dLacCer}{dt} = k_3 GlcCer$$

$$\frac{dGb_3}{dt} = k_4 LacCer_A$$

$$\frac{dGM_3}{dt} = k_5 LacCer_B$$

$$SM = Cer_{TOT} - Cer - LacCer - LacCer_A - LacCer_B - Gb_3 - GM_3$$

The reaction rates (k_1-k_5) were optimized using the MATLAB toolbox SBtoolbox2 in combination with SBPD [www.sbtoolbox2.org] and the local optimization method "SBsimplex". The best fit is obtained by minimizing an objective function, or Cost Function (CF), here chosen as the square of distances between experimental and simulated data points. In the initial simulation, all reaction rates were required to have the same value for mock-treated and FAPP2-KD cells (null hypothesis, N in **Supplementary Fig. 5b**). In subsequent simulations, the reaction rates were allowed to vary one at a time (from 0.01 to 10 fold with respect to the value assigned in N) between mock-treated and FAPP2-KD cells (**Supplementary Fig. 5b**). The lowest CF (0.019) was obtained when FAPP2 depletion was modelled to affect k_{3A}, i.e. GlcCer to LacCerA conversion. Thus, a reduction in k_{3A} (from 0.045 to 0.0063) is the change that best describes the overall effects of FAPP2-depletion on GSL metabolic fluxes. The simulation corresponding to this condition is shown in **Supplementary Fig. 5c**.

Localization of LCS and of GM3S in HeLa cells

We assessed whether the two distinct LacCer pools destined for GM3 or Gb3 synthesis were produced by the same LacCer synthase (LCS) or by different enzymes. As a first step we defined the molecular nature of LCS in HeLa cells as it has been reported that both the *B4GALT5* and *B4GALT6* genes encode LCSs[31]. We thus silenced the expression of the *B4GALT5* or the *B4GALT6* gene products in HeLa cells (**Supplementary Fig. 8a**) and assessed the effect of these treatments on GSL levels by ^{3}H-sphingosine pulse labelling for

24 hours. As shown in **Supplementary Fig. 8b**, B4GALT5 KD induced a nearly complete inhibition of LacCer and downstream GSL synthesis (both Gb3 and GM3, **Fig. 2f**, **Supplementary Fig. 8c, d**) while B4GALT6 KD did not. These results indicated that the two pools of LacCer are generated by the same LCS, *B4GALT5*, which, as assessed in immunoelectron microscopy (IEM) studies, is present both in the Golgi *cisternae* and in the TGN in cells expressing low levels of 3XFlag-B4GALT5 (**Supplementary Fig. 8c, d**).

We classified the HA-GM3S into low and high expressing cells (**Supplementary Fig. 9 b**) and chose the low-expressing cells for the morphological analysis of GM3S distribution (**Fig. 3b, c**). We observed that overexpressed HA-GM3S localized mainly in the Golgi *cisternae* when expressed at low levels (**Fig. 3b, c**), but also localized at the TGN when expressed at high levels (**Supplementary Fig. 9b, c**). We exploited this observation to challenge the hypothesis that the ability of FAPP2 to operate a *cis*-to-TGN shunt of GlcCer is required to feed a LacCer pool at the TGN that is used by TGN-resident, GSL-synthesizing enzymes. To this end, we isolated a stable HeLa cell clone expressing high levels of 3XHA-GM3S (HeLa-GM3S) where a significant fraction of GM3S resided in the TGN and asked whether GM3 synthesis required FAPP2. HeLa-GM3S produced approximately 7 times more GM3 than parental HeLa cells at the expense of Gb3 production (**Supplementary Fig. 9 c**), consistent with earlier reports[15]. In agreement with the ectopic localization of GM3S at the TGN seen by IEM in these cells, GM3 synthesis became sensitive to BFA treatment (**Supplementary Fig. 9d**), and interestingly, also to FAPP2 KD (**Supplementary Fig. 9e**), thus reinforcing the conclusion that the ability of FAPP2 to transfer GlcCer to the TGN is required for the activity of GSL synthesizing enzymes residing in this compartment.

Analysis of ARF-recruiting activity of the FAPP PH-E50A domain mutant

The E50A mutation has been shown to impair the binding of the FAPP1-PH domain to ARF1 in vitro[18]. We introduced the same mutation in the FAPP2-PH domain, expressed this GFP-FAPP2 PH-E50A in HeLa cells, and then evaluated its ability to bind ARF1 in intact cells exploiting our previous observation that, as a consequence of its ability to bind ARF1 and to compete with ARF-GAP1[14], FAPP-PH, in its tandem form, stabilizes ARF1 on Golgi

membranes[14]. We expressed the tandem forms of GFP-FAPP2 PH-E50A (diFAPP2-PH-E50A) and verified that, compared to diFAPP2-PH-wt, it had lost its ability to interact with ARF1 also in intact cells (**Supplementary Fig. 10a**).

Assessment of GlcCer loading of FAPP2

The GlcCer loading efficiency was measured by exploiting the presence of a key tryptophan (W407) in the putative FAPP2-GlcCer binding site, which is conserved compared to the glycolipid transfer protein GLTP[20]. As reported for GLTP[24] and for the GLTPH domain of FAPP2[20], GlcCer binding to full length FAPP2 induced a substantial decrease in tryptophan fluorescence intensity along with a shift of tryptophan fluorescence emission maxima towards lower wavelengths. No change was observed with the FAPP2-W407A mutant confirming that the observed effect was due to the quenching of W407-associated fluorescence (**Supplementary Fig. 11a**). We applied the procedure described in[24] to calculate the fraction of GlcCer-loaded FAPP2. In brief, the fraction of binding sites (α) occupied by C8-GlcCer was calculated by the equation

$$\alpha = (F - F0)/Fmax$$

where F0 and F are the W emission intensities of FAPP2 in the absence and presence of C8-GlcCer, respectively, and Fmax is the emission intensity of the fully liganded FAPP2, i.e. at excess C8-GlcCer. Fmax was determined by plotting 1/(F-F0) *vs.* 1/L and extrapolating 1/L = 0, where L equals the total glycolipid concentration. According to this procedure we concluded that more than 80% of FAPP2 GlcCer binding sites were occupied when a 1 to 1 FAPP2:GlcCer molar ratio was used, so this ratio was used for experiments in which we studied the impact of GlcCer loading on the interaction with PtdIns4*P* liposomes by SRP or for HDX-MS and controlled proteolysis experiments (**Fig. 4d, f, Supplementary Figures 12** and **13**). As a further and independent approach to assess the GlcCer loading of FAPP2, we analyzed the circular dichroism (CD) spectra of FAPP2 wt and FAPP2-W407A upon exposure to GlcCer and, in agreement with results obtained with the GLTP homology

domain of FAPP2[20], we observed that GlcCer induced a significant change in the CD profile of full length FAPP2wt, but not of full length FAPP2-W407A (**Supplementary Fig. 11b**).

Hydrogen-Deuterium exchange-Mass Spectrometry (HDX-MS)

10 µl of stock protein solutions (GST FAPP2 5 µM) were prepared in PBS with the addition of 10% glycerol. GlcCer was loaded by the dilution of a 1 mM stock in EtOH to a final concentration of 20 µM. Control experiments contained the same final concentration of EtOH. Exchange reactions were initiated by addition of 40 µl of a 98% D_2O solution containing 10 mM HEPES pH 7.2, 50 mM NaCl, and 2 mM DTT, giving a final concentration of 78% D_2O. Deuterium exchange reactions were allowed to carry on for five time periods, 3, 30, 300, 3000 seconds at 23 °C and 3 seconds at 0 °C. On-exchange was stopped by the addition of 20 µl of quench buffer containing 2.4% formic acid and 0.833 M guanidine-HCl, which lowered the pH to 2.6. Samples were then immediately frozen in liquid nitrogen until mass analysis.

Different digestion conditions were employed to optimize the peptide digestion map. These optimizations included changing denaturant concentration, flow rate over pepsin, and denaturation time. Peptide identification was performed by running tandem MS/MS experiments using a Xevo G2 Tof (Waters). Data was analyzed using Mascot software v. 2.2 (Matrix Science) to identify all peptides based on fragmentation and peptide mass (peptides with mascot scores >20 were examined), and these identifications were then manually validated using HD examiner software (Sierra Analytics) to test for correct m/z state, and the presence of overlapping peptides. Peptide mass tolerance was set at 10 ppm, with MS/MS tolerance of 0.1 Da.

Samples were thawed rapidly on ice and then injected onto an online HPLC system that was immersed in ice. The protein was run over an immobilized pepsin column (Applied Biosystems, Poroszyme®, 2-3131-00) at 50 µl/min, and collected over a 1.7 µm particle C18 peptide trap (2.1 mm x 8 mm, Waters Van-guard) for five minutes. The trap was then switched in line with a 1.7 µm particle, 1 mm x100 mm C18 column (Waters Acquity UPLC) with a vanguard pre-column, and peptides were eluted by a 5-45% gradient of buffer A (0.1% formic acid) and buffer B (100% acetonitrile) over 11 minutes and injected onto a Xevo G2 Tof (Waters) which collected mass spectra from a range of 300 to 1400 m/z. Mass

analysis of the peptide centroids was performed as described previously using the software HD examiner (Sierra Analytics)[26,32,33]. Briefly, all selected peptides passed the quality control threshold of the software, and were then manually examined for accurate identification and deuterium incorporation. Results are shown as relative levels of deuteration with no correction for back exchange as described previously[26,32,33]. The real level of deuteration will be ~25-35% higher than what is shown, based on tests performed with fully deuterated standard peptides. All experiments were repeated in triplicate, and we found that the average error was 0.18 Da. The resulting deuterium incorporation was graphed versus central number for each time point, along with the integrated difference between +/- GlcCer (**Supplementary Fig. 12** and **Fig. 4f**).

Controlled proteolysis and Mass spectrometry analysis of FAPP2 fragments

Aliquots of 50 µg of His-FAPP2 in its apo-form or in the GlcCer-bound form were digested separately with trypsin, using an enzyme-to-substrate ratio of 1:75 for 2 minutes. Samples of proteolysed FAPP2 were fractionated by SDS-PAGE and analyzed by Western blot using antibodies against the full length FAPP2 (anti-FAPP2) or directed against the C-terminus (anti C-Ter) (**Supplementary Fig. 13a, b**), and by Colloidal Coomassie (Pierce). Coomassie stained protein bands were excised and mapped by mass spectrometry following *in situ* tryptic digestion[34]. Peptide mixtures extracted from the gel were analyzed both by MALDIMS on a MALDI 4800 TOF-TOF (ABI SCIEX) and nano-chromatography tandem mass spectrometry (nanoLC-MS/MS) on a CHIP MS Ion Trap XCT Ultra equipped with a capillary 1100 HPLC system and a chip cube (Agilent Technologies, Palo Alto, CA). These analyses led to the identification of the different proteolysed forms of FAPP2 as reported in **Supplementary Fig. 13c** and indicated great flexibility of the unstructured region between the two domains, confirming the results from HDX-MS. Moreover, the higher level of the fragment 61-499 observed in the presence of GlcCer that originated from a proteolytic event within the PH domain suggested that binding of the ligand to the GLTPH domain increases the accessibility of the PH domain itself.

31 Nishie, T. *et al.* Beta4-galactosyltransferase-5 is a lactosylceramide synthase essential for mouse extra-embryonic development. *Glycobiology* **20**, 1311-1322, (2010).

32 Burke, J. E. *et al.* Dynamics of the phosphoinositide 3-kinase p110delta interaction with p85alpha and membranes reveals aspects of regulation distinct from p110alpha. *Structure* **19**, 1127-1137, (2011).

33 Burke, J. E. & Williams, R. L. Dynamic steps in receptor tyrosine kinase mediated activation of class IA phosphoinositide 3-kinases (PI3K) captured by H/D exchange (HDX-MS). *Advances in biological regulation*, (2012).

34 Troise, F. *et al.* A novel ErbB2 epitope targeted by human antitumor immunoagents. *FEBS J* **278**, 1156-1166.

35 Breggia, A. C. & Himmelfarb, J. Primary mouse renal tubular epithelial cells have variable injury tolerance to ischemic and chemical mediators of oxidative stress. *Oxid Med Cell Longev* **1**, 33-38, (2008).

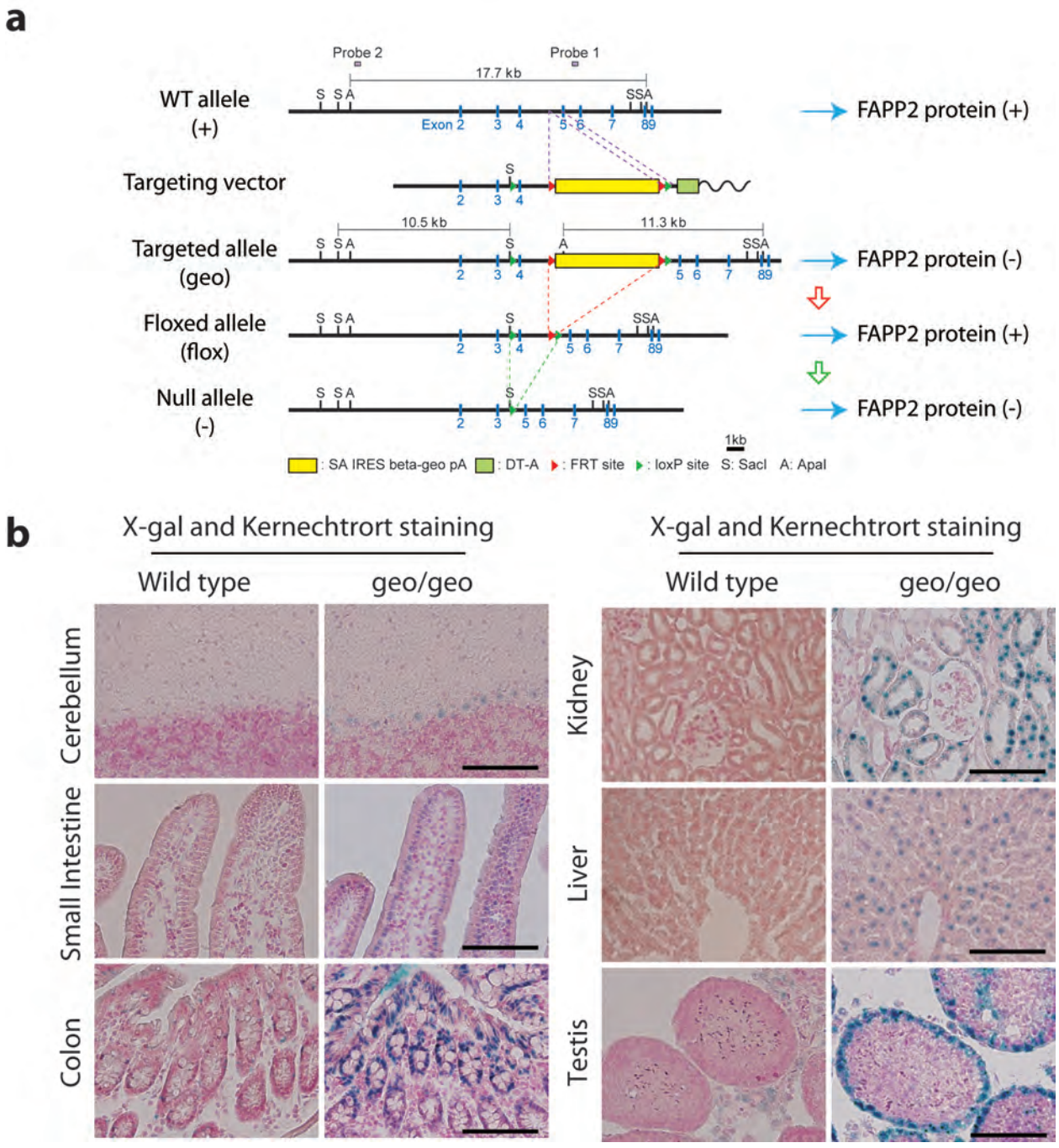

Supplementary Figure 1: Establishment and characterization of FAPP2-/- mice
(**a**) Restriction maps of wild-type FAPP2 allele (+), targeting vector, targeted allele (geo), floxed allele obtained by crossing with Flp transgenic mice (flox), and the null FAPP2 allele (-) obtained after Cre-mediated excision of exon 4 (see Supplementary data). (**b**) Distribution of FAPP2 as assessed by X-Gal and Kernechtrort staining in the indicated tissues from FAPP2geo/geo 8-to-10-week-old mice. Bars, 100 μm.

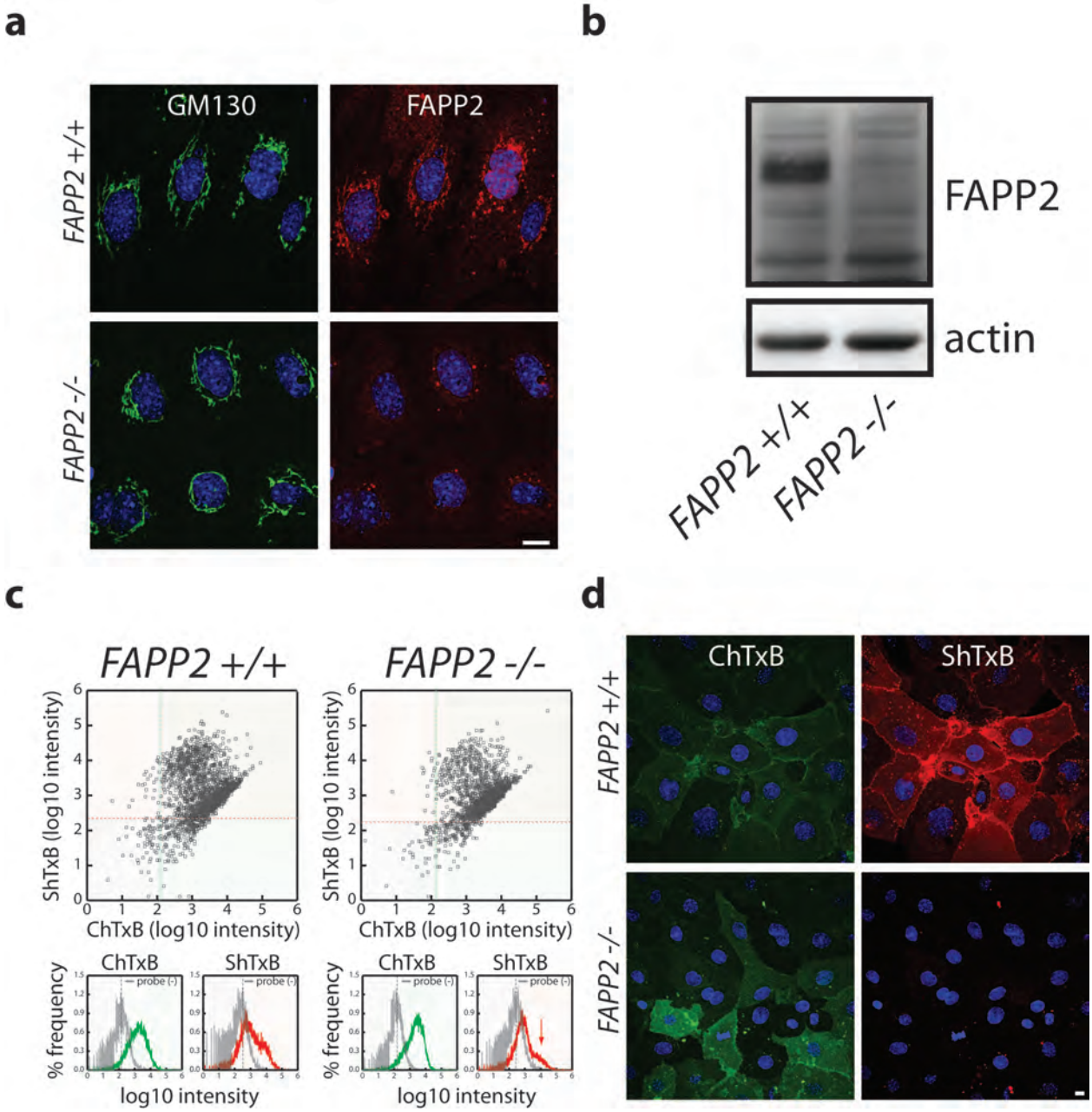

Supplementary Figure 2: Gb3 and GM1 expression in isolated kidney tubular cells from wt and FAPP2 -/- mice. Kidney tubular cells were isolated according to the procedure described in[35] and (**a**) stained with anti-GM130 antibodies (green) and anti-FAPP2 (red) antibodies. (**b**) Western Blot analysis of lysates from Kidney cells. (**c**) FACS analysis of isolated tubular kidney cells double stained with fluorescently labelled ChTxB, and ShTxB, (upper panels). Dotted lines indicate threshold values for background staining. The lower panels show the frequency of ChTxB- (green) or ShTxB- (red) positive cells. The arrow indicates the selective reduction in the frequency of ShTxB positive cells. (**d**) Immunofluorescence of isolated tubular kidney cells double stained with ChTxB (green) or ShTxB (red). Bars; 10 μm.

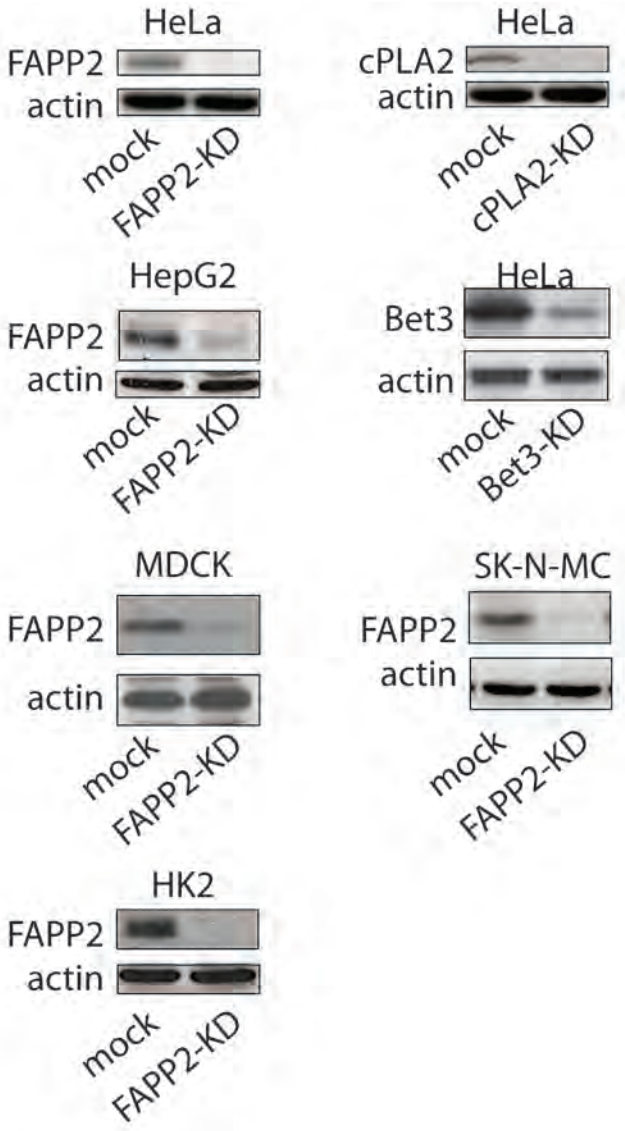

Supplementary Figure 3: Protein down-regulation after siRNA treatments.
The proteins FAPP2, Bet3, and cPLA2 were detected using specific antibodies in the indicated mock- or siRNA-treated (KD) cells (HeLa, MDCK, HK2, SK-N-MC). Actin was taken as an internal control protein. The sequences of the different siRNAs are reported in **Supplementary Table 1**.

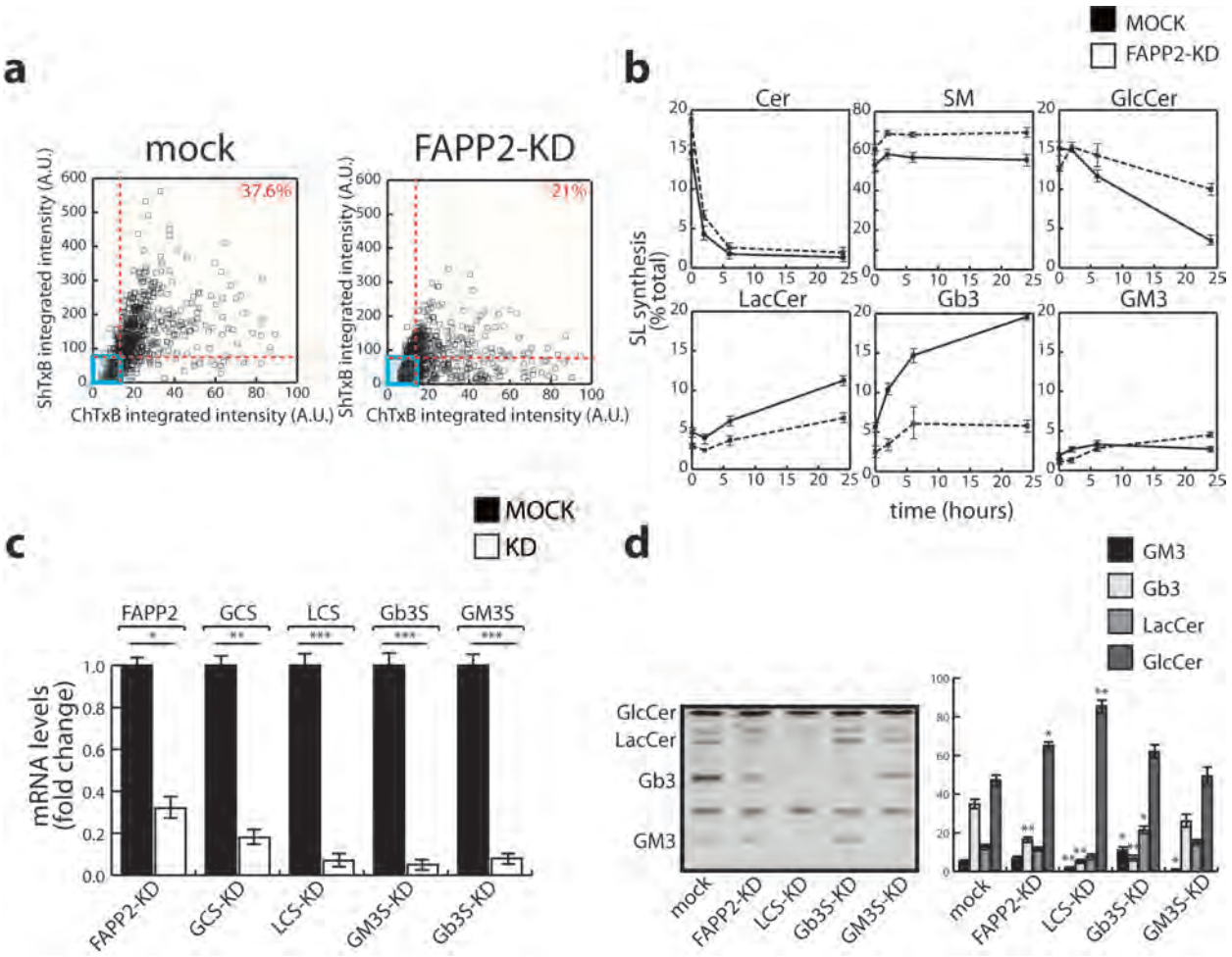

Supplementary Figure 4: FAPP2 selectively controls Gb3 synthesis

(**a**) A HeLa cell population expressing both Gb3 and GM1 at levels detectable by ShTxB and ChTxB, respectively, was selected by FACS (mock) and then subjected to treatment with FAPP2 siRNA (FAPP2-KD). The blue box delimits values of ShTxB and ChTxB staining corresponding to background staining. Numbers indicate the percentage of double-positive cells. The decrease in this percentage induced by FAPP2-KD is statistically significant ($p<0.001$) and is paralleled by the increase in the percentage of cells that express only GM1 (from 16% to 28%). (**b**) Pulse-chase-HPTLC analysis of mock-treated or FAPP2-KD HeLa cells, pulsed with ^{3}H-sphingosine for 2h and chased for 0, 2, 6, and 24h. Results are the means of at least 3 independent experiments ± SEM. (**c, d**) Comparison of the effects on GSL levels induced by silencing the different GSL synthetic enzymes or FAPP2 (**c**) RT-qPCR-based assessment of siRNA-mediated silencing of genes involved in GSL synthesis (see Supplementary **Tables 1** and **2**). GCS, GlcCer synthase; LCS, LacCer synthase; GM3S, GM3 synthase; Gb3S, Gb3 synthase. (**d**) Effects of siRNA-mediated silencing of the indicated genes on GSL synthesis assessed in cells labelled with C12-BODIPY-GlcCer for 3 hours. Values indicate the percentage of C12-BODIPY-GlcCer incorporated into each given GSL compared to the total GSLs.

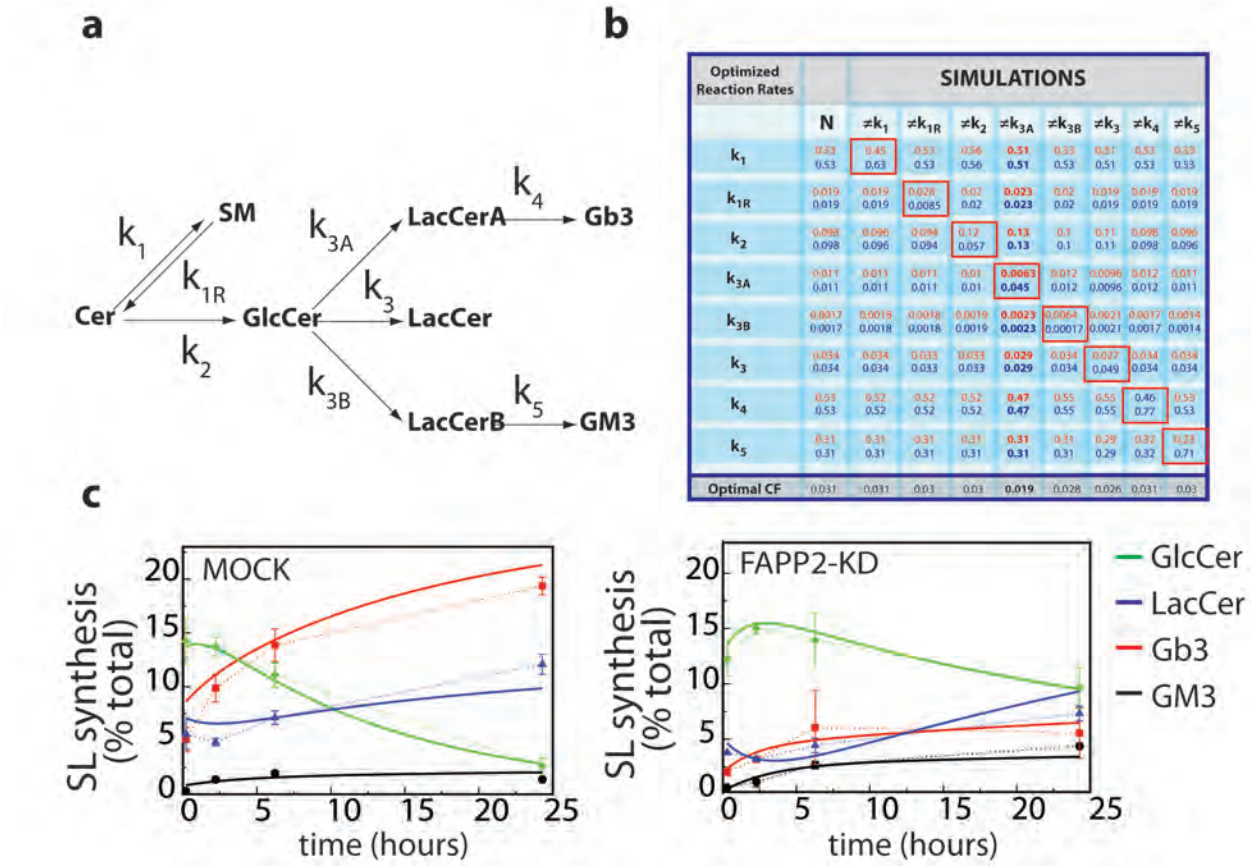

Supplementary Figure 5: Mathematical modelling of GSL metabolic fluxes in control and FAPP2 KD cells

(**a**) Reactions and reaction rates considered in the mathematical modelling of the experimental data shown in **Supplementary Fig. 4a**. (**b**) Optimized reaction rates and Cost Functions (CF) under different simulation conditions in which the reaction rates were either required to be all equal (null hypothesis, N) or were allowed to vary one at a time (red boxed cells) between mock-treated (blue) and FAPP2 KD cells (red). The reaction rates extracted from the simulation leading to the lowest CF are indicated in bold and were used for the metabolic model shown in (**c**). In (**c**) dotted lines refer to experimental data, continuous lines represent the best fit obtained from mathematical modelling (see also **Supplementary Data**).

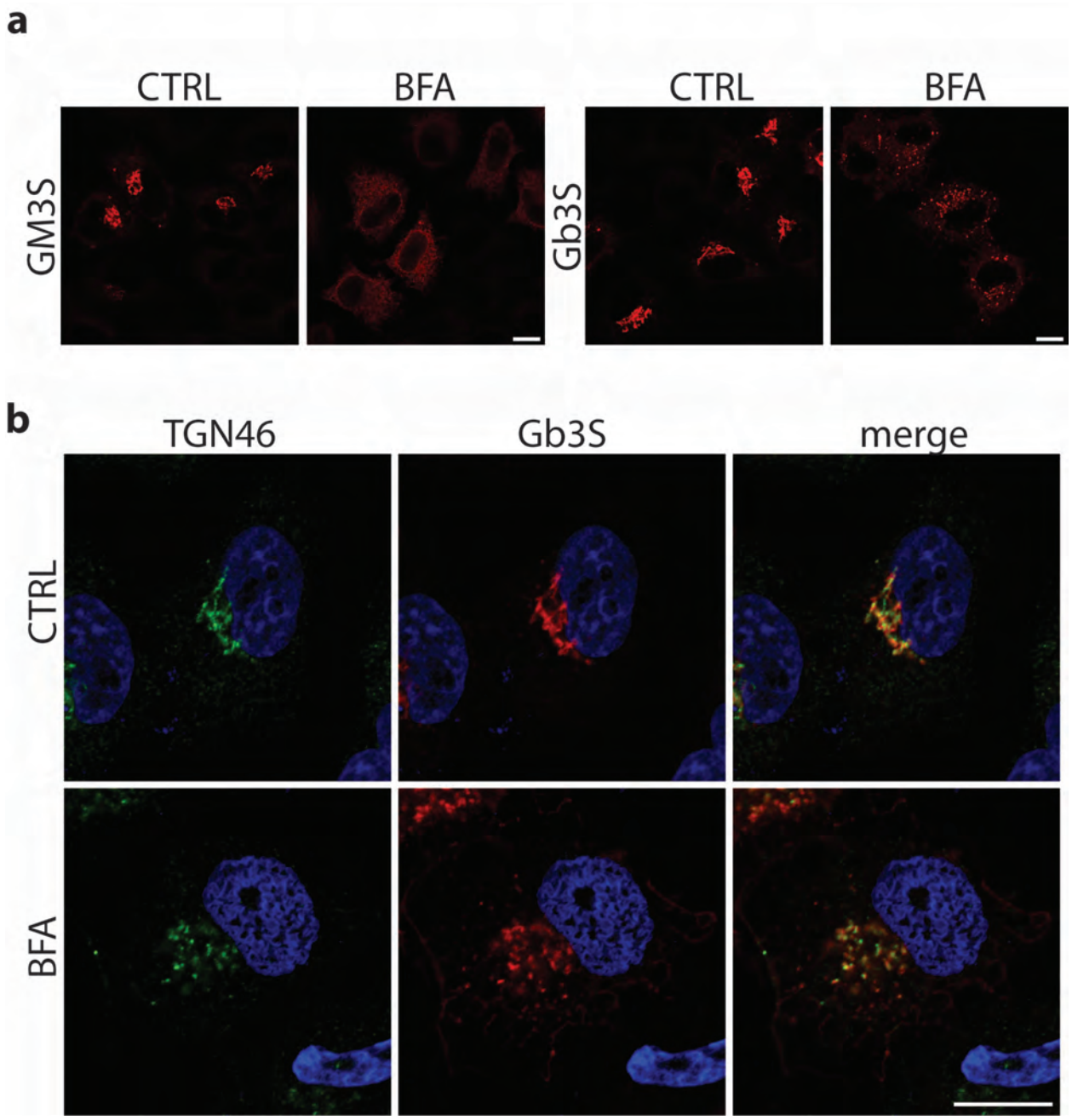

Supplementary Figure 6: **Effect of BFA on 3XHA–Gb3S and 3XHA–GM3S distribution.** (**a**) Immunofluorescence showing localization of GM3S and Gb3S at steady state (CTRL) and upon BFA treatment (5μg/ml 30 min) (BFA). (**b**) Immunofluorescence showing Gb3S, TGN46 and their co-localization after BFA treatment (merge). Bars; 10 μm.

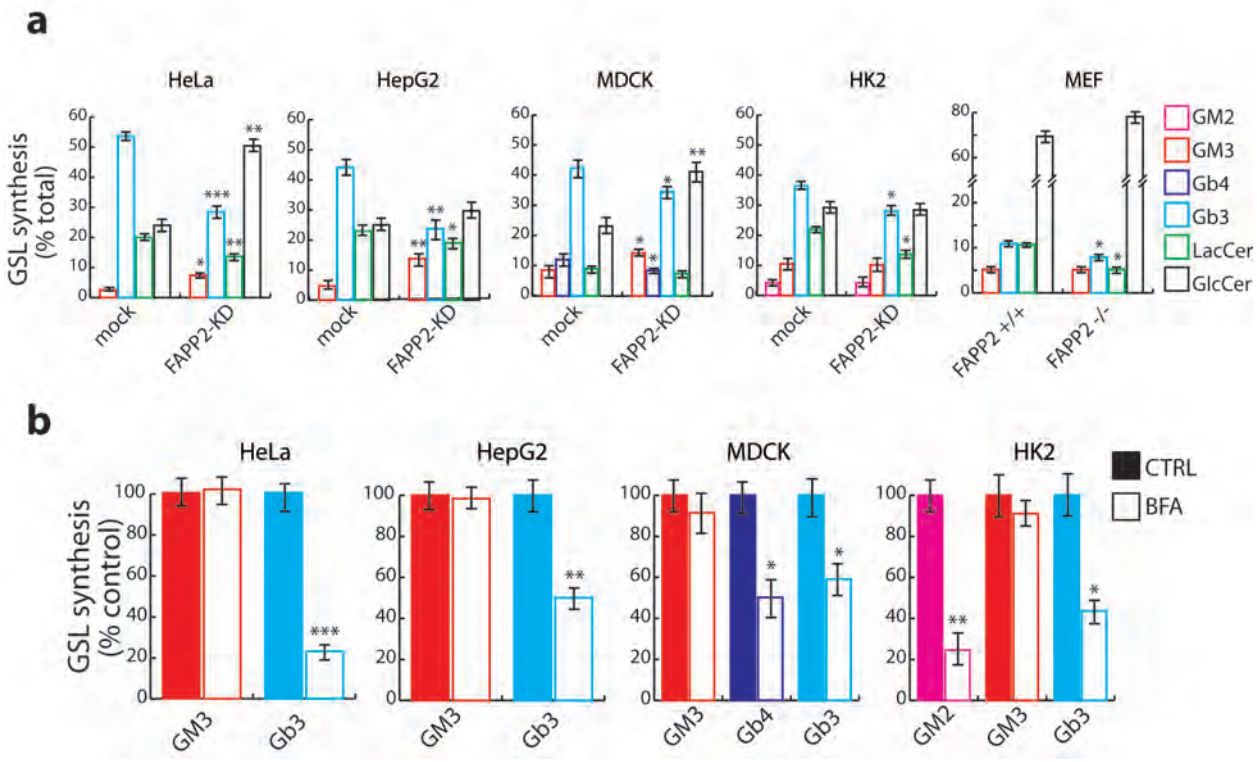

Supplementary Figure 7: FAPP2 controls the synthesis of globosides at the TGN in different cell lines. (**a**) Effect of FAPP2-KD on GSL synthesis in different cell lines (HeLa, MDCK, HepG2, HK2). Also shown (last bar graph) are the GSLs synthesized in mouse embryo fibroblasts (MEF) from wt and FAPP2-/- mice. GSL synthesis was assessed by ^{14}C-galactose (HeLa, MDCK, HepG2) or ^{3}H-sphingosine (HK2, MEF) labelling (6 hours). (**b**) Effect of BFA on GSL synthesis in the indicated cell lines (HeLa, MDCK, HepG2, HK2 cells). GSL synthesis was assessed by ^{3}H-sphingosine or ^{14}C-galactose (MDCK) labelling (3 hours). Asterisks indicate statistically significant differences with control or untreated cells. * p<0,05; ** p< 0,01; *** p<0.001.

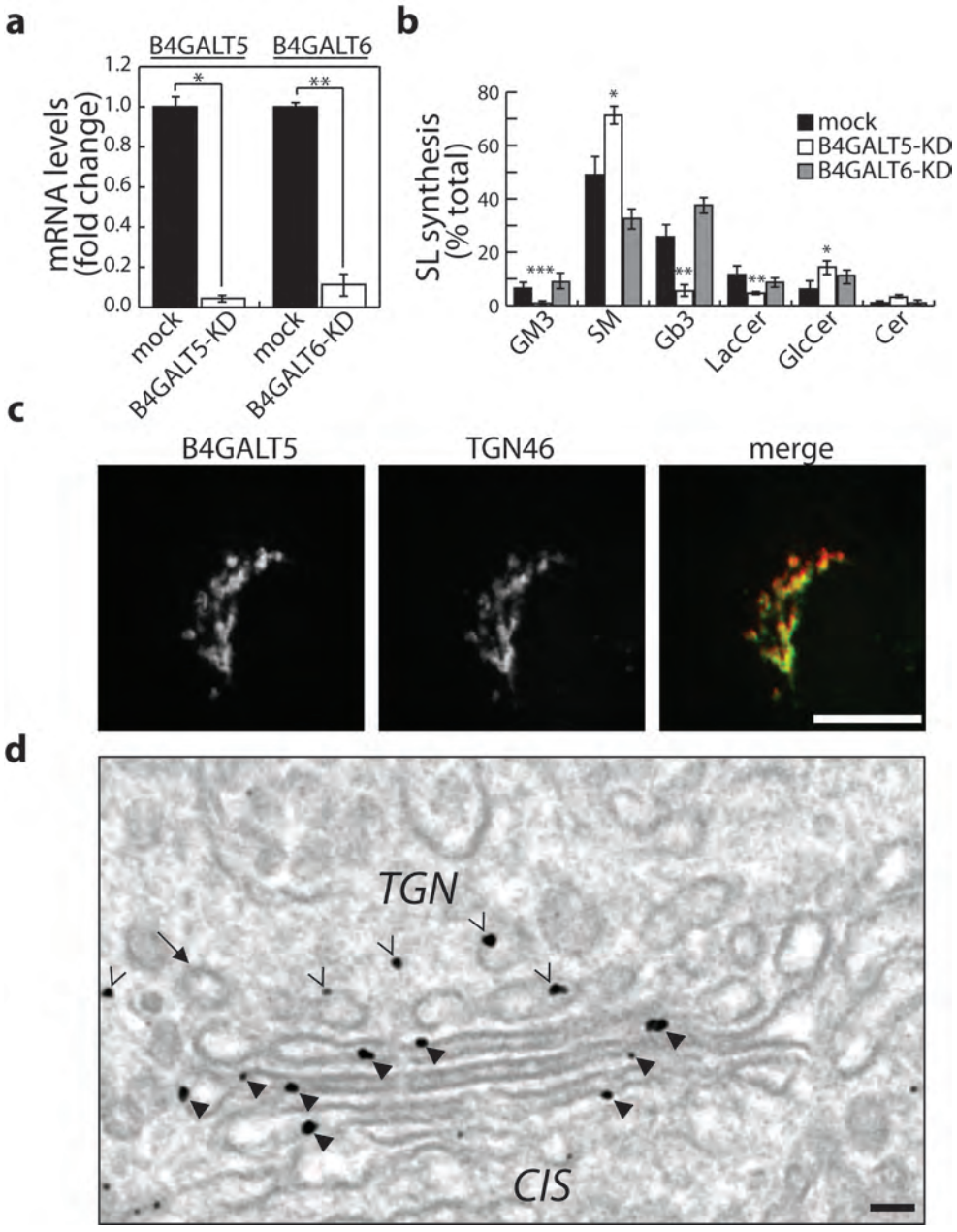

Supplementary Figure 8: **B4GALT5, the LacCer synthase in HeLa cells, is localized both in the Golgi *cisternae* and in the TGN**

(**a**) Graph showing the efficiency of B4GALT5 and B4GALT6 KD following specific siRNA treatment as estimated by RT-qPCR. (**b**) Effect of B4GALT5 KD and B4GALT6 KD on sphingolipid levels in HeLa cells labelled with ^{3}H-sphingosine for 24 hours. (**c**) Localization of B4GALT5 assessed by immunofluorescence in comparison with a TGN marker (TGN46). (**d**) Localization of B4GALT5 assessed by IEM. Black arrowheads indicate B4GALT5 localized in the Golgi, wedges indicate B4GALT5 localized in the TGN; the black arrow points to a clathrin-coated round profile, indicative of the TGN. Bars (**c**)=10 μm; (**d**)=100 nm.

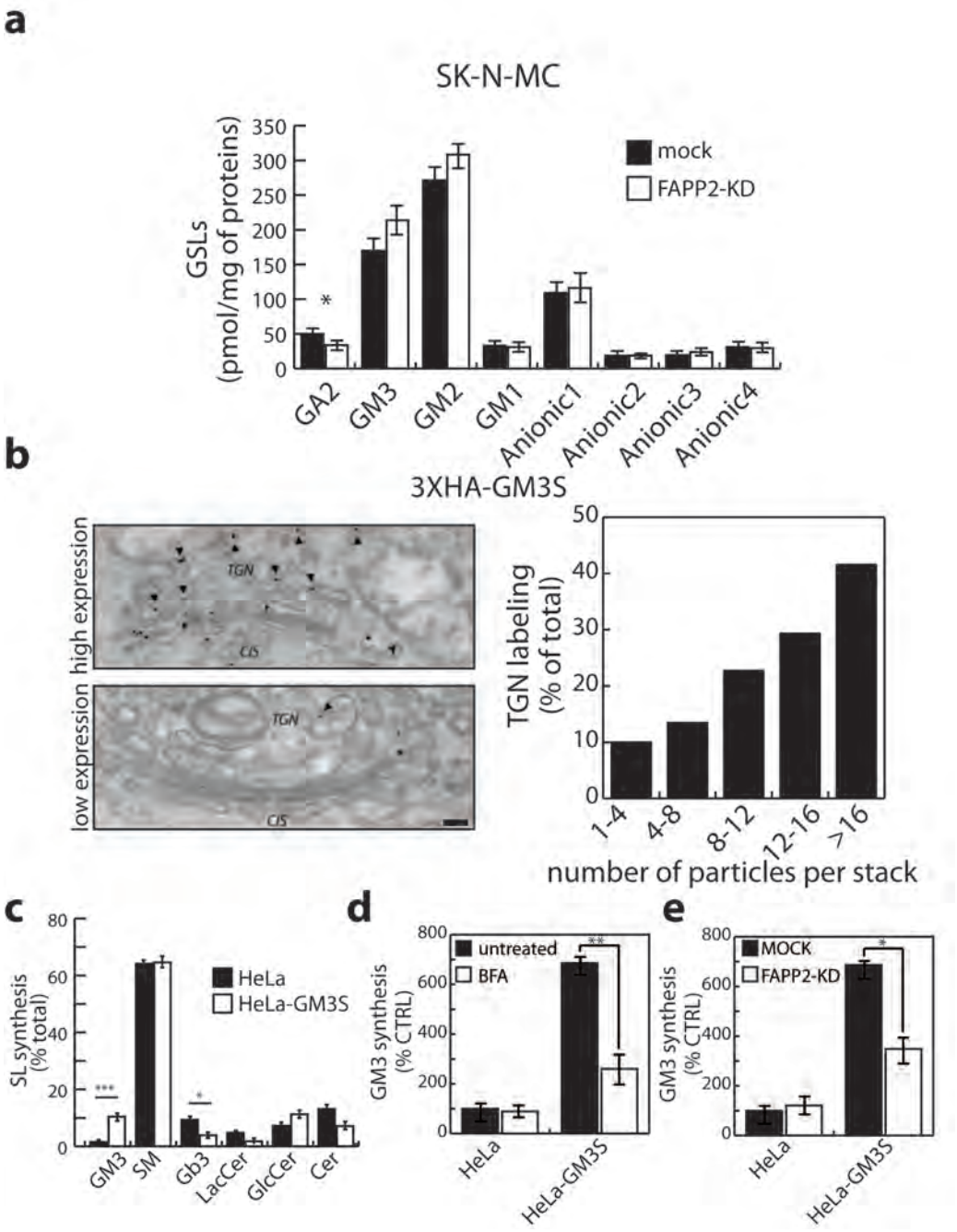

Supplementary Figure 9: FAPP2 is selectively required for TGN-located enzymes that act on LacCer to make complex GSLs.

(**a**) Effect of FAPP2-KD on GSL levels assessed by HPLC analysis in SK-N-MC neuronal cells. (**b-e**) Ectopic expression of GM3S at the TGN renders GM3 synthesis sensitive to FAPP2 depletion: (**b**) Localization of 3XHA-GM3S in cells expressing different amounts of the protein. Left, IEM of Golgi stacks from cells expressing low levels (lower panel) or high levels (upper panel) of 3XHA-GM3S. Arrowheads point to TGN-localized staining. Quantitative analysis of the TGN localization of 3XHA-GM3S in relation to the levels of expression. (**c**) Sphingolipid synthesis in HeLa cells overexpressing GM3S (HeLa-GM3S) in comparison to parental HeLa cells as assessed by a 3h pulse with ^{3}H-sphingosine. (**d**) Effect of BFA treatment (5μg/mL) on HeLa cells overexpressing GM3S (HeLa-GM3S) in comparison to parental HeLa cells. Values are expressed as percent of control (CTRL) taken as untreated parental HeLa cells. (**e**) Effect of FAPP2-KD on GM3 synthesis (3 hours ^{3}H-sphingosine pulse) in HeLa cells overexpressing GM3S (HeLa-GM3S) compared to parental HeLa cells. Values are expressed as percent of control (CTRL) taken as mock-treated parental HeLa cells.

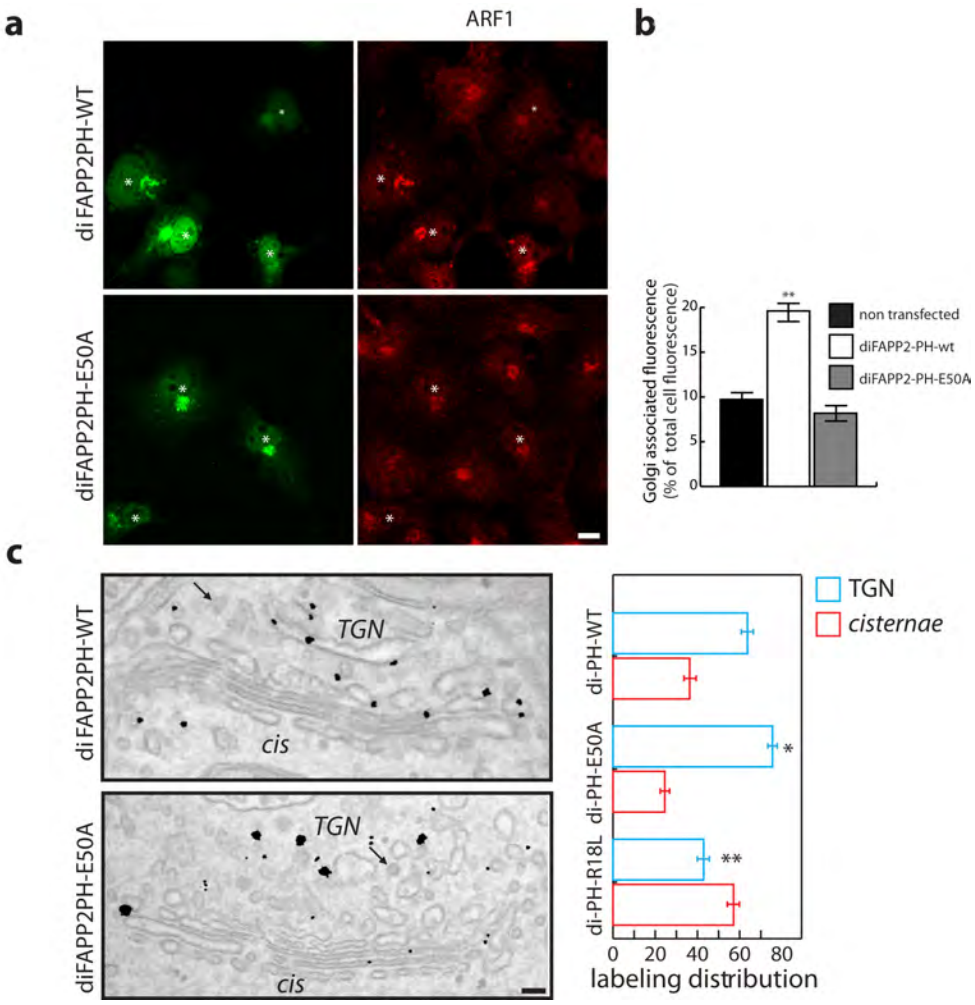

Supplementary Figure 10: PtdIns4*P* drives the localization of FAPP2 PH at the TGN
(**a**) The E50A mutant of the FAPP2-PH domain does not stabilize ARF1 on the Golgi complex**.** Cos7 cells transfected with plasmids encoding GFP-tagged diFAPP2-PH wt or E50A, a mutant in the ARF1 binding site[18], were processed for indirect immunofluorescence with anti-ARF1 antibodies. Asterisks indicate transfected cells. Bar, 10 µm. (**b**) Quantification of the stabilization of ARF1 on the Golgi complex was evaluated as percentage of Golgi-associated ARF1-fluorescence to total ARF1 fluorescence. (**c**) Tandem PH domains of FAPP2 in the wt form (diPH wt, which can bind both ARF and PtdIns4*P*) or in the E50A mutant form (diPH-E50A, which cannot bind ARF, see above (**a**) and [18], or in the R18L form (diPHR18L, which cannot bind PtdIns4*P* [14], were expressed as GFP chimerae and their intra-Golgi distribution was analyzed by immunoelectron microscopy (Bar, 100nm). Black arrows point to clathrin-coated profiles, which are indicative of the TGN. Right panel shows the quantification of TGN- and *cisternae*-associated particles. Data are means ± S.E.M. of at least 30 stacks analyzed per condition.

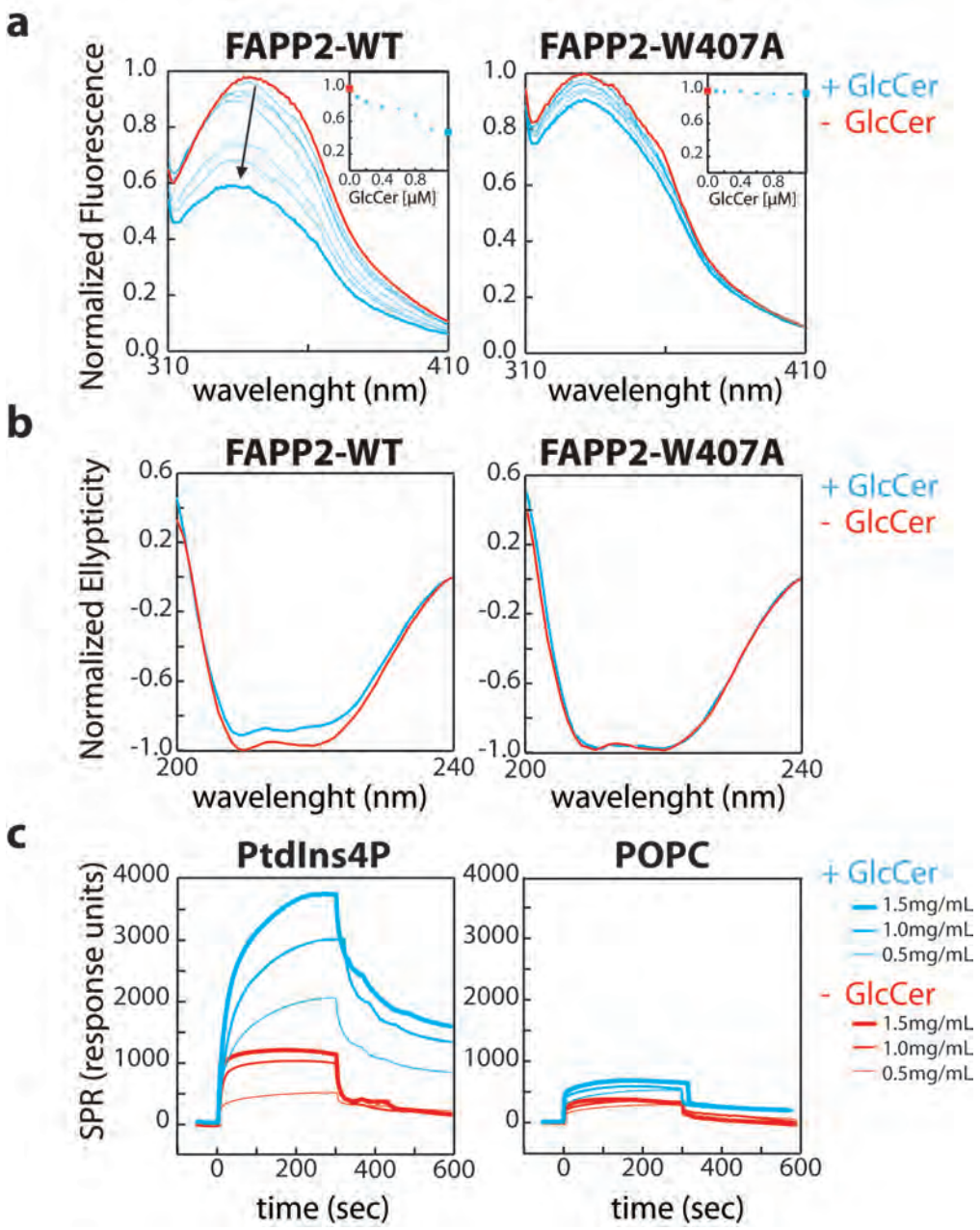

Supplementary Fig.11: Effect of GlcCer binding on FAPP2 conformation
(**a**) Assessment of GlcCer loading of FAPP2. GlcCer induces a shift of the tryptophan fluorescence in FAPP2; cyan lines indicate tryptophan fluorescence at increasing concentrations of C8-GlcCer (from 0 to 1.2 µM, as detailed in the inset); the arrow indicates the change in tryptophan fluorescence maximal emission; the inset shows the effect of increasing concentrations of C8-GlcCer on tryptophan maximal emission. (**b**) Effect of C8-GlcCer loading on recombinant FAPP2-wt and FAPP2-W407A circular dichroism. (**c**) Effect of C8-GlcCer loading on FAPP2 affinity for POPC or POPC and PtdIns4*P*-containing liposomes as measured by Surface Plasmon Resonance. Increasing concentrations of FAPP2 (ranging from 0.5 to 1.5 mg/mL) in its apo-form or loaded with equimolar amount of C8-GlcCer, were used. Results are representative of at least three independent experiments

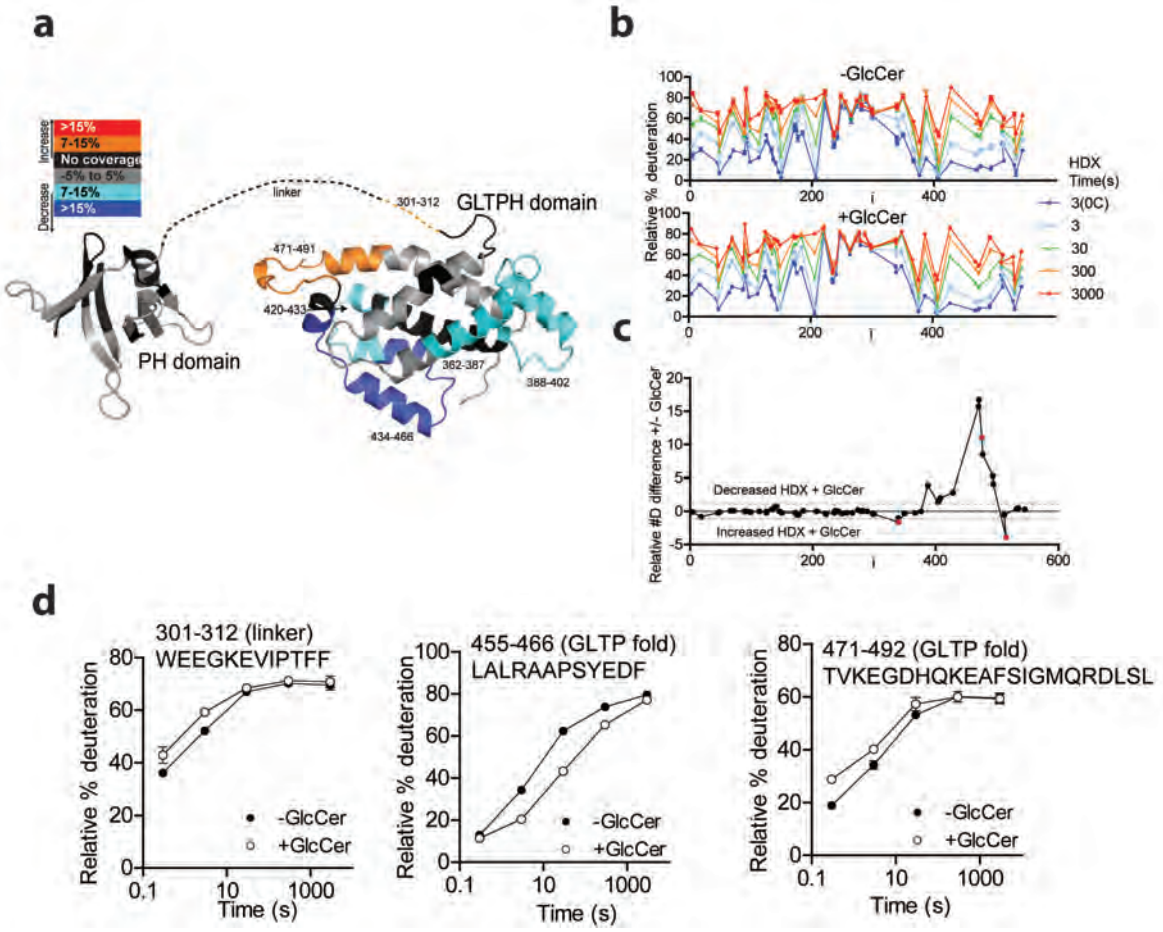

Supplementary Figure 12: GlcCer loading induces conformational changes in FAPP2: HDX-MS of FAPP2 in the presence and absence of GlcCer.

(**a**) The areas that are differently exposed to deuterium exchange in the presence or absence of GlcCer are indicated according to the reported colour code. (**b**) Global percentage of HDX is shown in the presence and absence of GlcCer for all peptides graphed according to their central residue number (i). All experiments were performed in triplicate and SD is shown on the graph. (**c**) The integrated difference in the number of deuteriums incorporated at all time points between FAPP2 +/- GlcCer are graphed according to their central residue number (i). Dotted lines indicate an integrated difference of either plus one or minus one incorporated deuterons. Three selected peptides with differences in exchange are highlighted as red dots and their plots of deuterium incorporation over time are shown in (**d**).

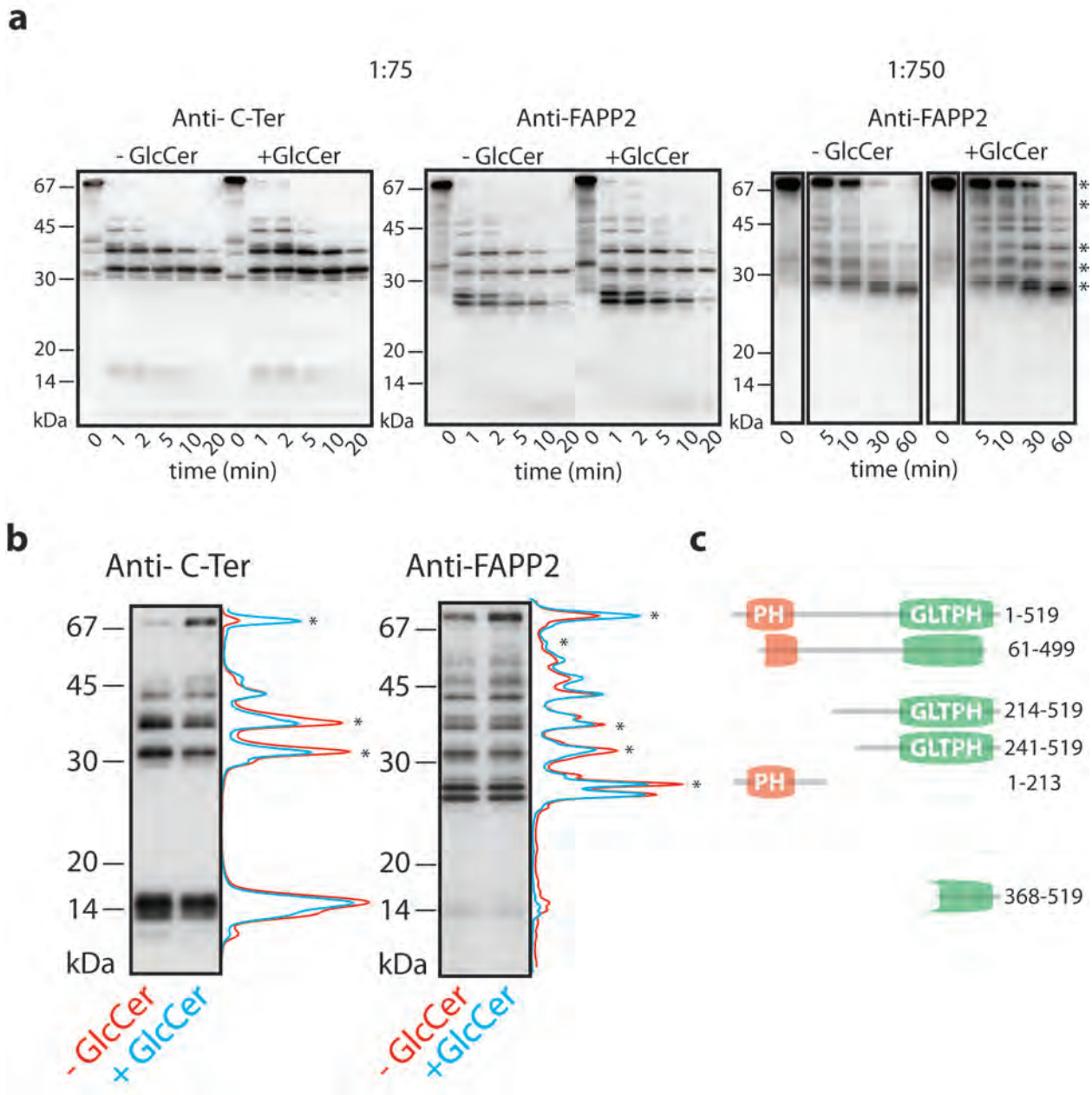

Supplementary Figure 13: GlcCer loading induces conformational changes in FAPP2: Controlled proteolysis studies on apo-FAPP2 and GlcCer-bound FAPP2.
Apo- or GlcCer-bound FAPP2 were subjected to controlled proteolysis (see **Supplementary methods**) (treatment with trypsin in molar ratio 1:75 or 1:750, as indicated for the indicated times at 37°C). (**a, b**) The samples were analyzed by Western blot with two different anti-FAPP2 antibodies, directed against the C-terminus (anti-C-Ter) or against the full-length FAPP2 protein (anti-FAPP2). In (**b**) the peptides that show differential sensitivity to trypsin treatment in the absence or presence of GlcCer are indicated with an asterisk. The digested samples were also analyzed by mass-spectrometry (as detailed in **Supplementary data**) and the protein fragments inferred from the identified peptides are shown on the schematic drawing of the FAPP2 protein in (**c**).

Supplementary Table 1

name	siRNA sequence
FAPP2.1	GAGAUAGACUGCAGCAUAU[dT][dT]
FAPP2.2	GAAUUGAUGUGGGAACUUU[dT][dT]
FAPP2.3	GAAAUCAACCUGUAAUACU[dT][dT]
FAPP2.4	CCUAAGAAAUCCAACAGAA[dT][dT]
GSC.1	GAUAUGAAGUUGCAAAGUA[dT][dT]
GSC.2	GCGAAUCCAUGACAAUAUA[dT][dT]
GSC.3	GGACCAAACUACGAAUUAA[dT][dT]
GSC.4	GAUGCUAGAUUGUUUAUAG[dT][dT]
B4GALT5.1	GUGAAAUUGGAAUGGAUUA[dT][dT]
B4GALT5.2	GCUUAACAGUGGAACAAUU[dT][dT]
B4GALT5.3	GGAAAGUGAUCGCAACUAU[dT][dT]
B4GALT6.1	CAUAUCUCUUUAUGGUACA[dT][dT]
B4GALT6.2	CUCCAAUCGAAGACUAUUA[dT][dT]
B4GALT6.3	GGUAUUCCAAGGAGCGUCA[dT][dT]
SIAT9.1	CAAUGGCGCUGUUAUUUGA[dT][dT]
SIAT9.2	GACCAUGCAUAAUGUGACA[dT][dT]
SIAT9.3	CGGAAGUUCUCCAGUAAAG[dT][dT]
SIAT9.4	AGGAAUACUGCACGGAUUA[dT][dT]
A4GALT.1	AGAAAGGGCAGCUCUAUAA[dT][dT]
A4GALT.2	GGACACGGACUUCAUUGUU[dT][dT]
A4GALT.3	UGAAAGGGCUUCCGGGUGG[dT][dT]
A4GALT.4	GCACUCAUGUGGAAGUUCG[dT][dT]
PLA2.1	GGACAGUCGUUAAGAAGUA[dT][dT]
PLA2.2	GGAGAAACACUAAUUCAUA[dT][dT]
PLA2.3	GGAGAAGACUUUCAGACAA[dT][dT]
PLA2.4	GUACAAGGCUCCAGGUGUU[dT][dT]
Bet3.1	GAUAACCACUCAUCCCUUA[dT][dT]
Bet3.2	GGGCAUCACUCCAAGCAUU[dT][dT]
Bet3.3	GAAAGGAGACGGUGUGACA[dT][dT]
Bet3.4	GGAAACUGCGGAUGUCAUU[dT][dT]
cFAPP2.1	GAACUACUCUAUCGUACUC[dT][dT]
cFAPP2.2	GAGAGGACAACCUGGGAAA[dT][dT]
cFAPP2.3	GCAAAUGGAGUUAAACAGU[dT][dT]
cFAPP2.4	GCCAAGAAAUCAUCCCAAC[dT][dT]

Sequences of the siRNA oligonucleotides used in this study.

cFAPP2.1-4 indicate canine FAPP2 si RNAs used to knock down FAPP2 in MDCK cells

Supplementary Table 2

name	Oligo sequence
βACTIN(+)	AAGAGCTACGAGCTGCCTGA
βACTIN(-)	GACTCCATGCCCAGGAAGG
HPRT1(+)	TGCTGACCTGCTGGATTACA
HPRT1(-)	CCTGACCAAGGAAAGCAAAG
B4GALT5(+)	CAATCGGTGCTCAGGTTTATG
B4GALT5(-)	GGTTTCACTGTGGTTCAAGTC
B4GALT6(+)	TCCTAAGTCTCCCTCTGGTC
B4GALT6(-)	ACGTATCTCCCGGAAAACTTC
FAPP2(+)	GGAGGGGGTGCTGTACAAGT
FAPP2(-)	GGACAATATTCCCCCACAGA
A4GALT(+)	GATCCCCACCTCTCTGCAAT
A4GALT(-)	TTGGACATGGTATCCCCAGA
SIAT9(+)	TGGTTATTGGAAGCGGAGG
SIAT9(-)	TCTGAATATCCCTCAACTGGTG
GCS(+)	TTCGGGTTCGTCCTCTTC
GCS(-)	GCTTGCTATAAGGCTGTTTGTC

Sequences of the rt-qPCR primers used in this study